Global and Seasonal Assessment of Interactions between Climate and Vegetation Biophysical Processes: A GCM Study with Different Land–Vegetation Representations

YONGKANG XUE

Department of Geography, and Department of Atmospheric and Oceanic Sciences, University of California, Los Angeles, Los Angeles, California

FERNANDO DE SALES

Department of Geography, University of California, Los Angeles, Los Angeles, California

RATKO VASIC

Department of Geography, University of California, Los Angeles, Los Angeles, California, and NOAA/NCEP, Camp Springs, Maryland

C. ROBERTO MECHOSO AND AKIO ARAKAWA

Department of Atmospheric and Oceanic Sciences, University of California, Los Angeles, Los Angeles, California

STEPHEN PRINCE

Department of Geography, University of Maryland, College Park, College Park, Maryland

(Manuscript received 26 January 2009, in final form 15 July 2009)

ABSTRACT

A global and seasonal assessment of regions of the earth with strong climate–vegetation biophysical process (VBP) interactions is provided. The presence of VBP and degree of VBP effects on climate were assessed based on the skill of simulations of observed global precipitation by two general circulation models of the atmosphere coupled to three land models with varying degrees of complexity in VBP representation. The simulated VBP effects on precipitation were estimated to be about 10% of observed precipitation globally and 40% over land; the strongest impacts were in the monsoon regions. Among these, VBP impacts were highest on the West African, South Asian, East Asian, and South American monsoons. The specific characteristics of vegetation–precipitation interactions in northern high latitudes were identified. Different regions had different primary impact season(s) depending on regional climate characteristics and geographical features. The characteristics of VBP effects on surface energy and water balance as well as their interactions were also analyzed. The VBP-induced change in evaporation was the dominant factor in modulating the surface energy and water balance. The land–cloud interaction had substantial effects in the feedback. Meanwhile, the monsoon regions, mid-latitudes lands, and high-latitude lands each exhibited quite different characteristics in circulation response to surface heating changes. This study is the first to compare simulations with observations to identify and assess global seasonal mean VBP feedback effects. It is concluded that VBPs are a major component of the global water cycle.

Corresponding author address: Yongkang Xue, Department of Geography, 1255 Bunche Hall Box 951524, UCLA, Los Angeles, CA, 90095.
E-mail: yxue@geog.ucla.edu

DOI: 10.1175/2009JCLI3054.1

1. Introduction

The recent Intergovernmental Panel on Climate Change (IPCC) report (Bates et al. 2008) has shown that freshwater resources can be strongly impacted by climate change, with wide-ranging consequences for human societies and ecosystems. Understanding the role of land surface in the water cycle is crucial in projecting future climate change and evaluating the impact on water resources since landscapes may face tremendous modifications in the coming centuries owing to land use changes and global warming. The importance of land surface processes in the climate system has been mostly supported by studies on climate sensitivity to albedo (i.e., Charney et al. 1977; Sud and Fennessy 1982; Dirmeyer and Shukla 1994), soil moisture (i.e., Shukla and Mintz 1982; Hong and Kalnay 2000; Douville et al. 2001; Koster et al. 2006), other individual land variables such as surface roughness (Sud et al. 1988) and leaf area index (LAI) (i.e., Chase et al. 1996; Kang et al. 2007), and some combinations of these variables (i.e., Yasunari et al. 2006). In addition, the effects of land cover changes have also been tested for several specific regions, such as Amazonia (i.e., Dickinson and Henderson-Sellers 1988; Nobre et al. 1991; Avissar and Werth 2005), the Sahel (i.e., Xue and Shukla 1993; Xue 1997), boreal forest (Bonan et al. 1992), and East Asia (i.e., Xue 1996; Fu et al. 2004), as well as for global vegetation types (e.g., Kleidon et al. 2000; Zhao et al. 2001; Snyder et al. 2004). In these studies, the effects of two different values of key surface variables, such as albedo, or two different surface conditions—for example, potential or degraded vegetation types—have been assessed using climate models. Two quite extreme values of the conditions/variables were usually assigned in order to highlight potential interactions. Recently, effects of feedbacks of dynamic vegetation on the West African climate and terrestrial carbon cycle have been tested at decadal and century scales (Claussen 1997; Wang and Eltahir 2000; Zeng et al. 1999; Cox et al. 2000; Notaro et al. 2005). In most of these studies, no observational data were used to evaluate results. So far, the investigation of land processes effects has been carried out in highly idealized frameworks. In general, sensitivity and feedback mechanisms were their major foci. Interaction between vegetation and climate is a dynamic process, involving many feedbacks, and is not a simple linear summation of the independent effects of individual surface processes. A global assessment of vegetation effects on the climate system in reference to observational data has not been conducted as indicated above. Consequently, the global and temporal characteristics of vegetation biosphysical processes (VBP)–climate interactions remain poorly understood. The uncertainties and shortcoming in simulating VBP effects with climate models undermine the credibility of their predictions of climate change and, in particular, of the role of human activities in changing climate. We use ''VBP'' here to specify those land surface processes relevant to climate interactions associated with vegetation since the term ''land surface process'' in climate modeling has been loosely applied to many individual components in the terrestrial surface, such as albedo and soil moisture. In the present study we employ observational precipitation data in a modeling study to provide a first preliminary global and seasonal assessment of VBP effects on the water cycle. The assessment was conducted at the global scale (i.e., is not limited to one or two regions) in recognition of the strong interconnections between regional climates, and covers all seasons (i.e., is not limited to the summer). The impact at long temporal scales, however, is not addressed in this study. VBPs include (but are not limited to) radiative transfer in the canopy, moisture exchange between soil layers and extraction by roots, canopy transpiration due to stomatal control, water interception loss, and drag effects due to vegetation morphology (i.e., Sellers et al. 1986; Xue et al. 1991; Dickinson 1992; Bonan 2008). A fundamental and comprehensive understanding of VBP effects in the climate system, for example, identifying regions and seasons where VBPs exert strong climate impact, is crucial to understand and assess roles of land–atmosphere feedback in the present and future climate.

Assessing VBP effects in the climate system requires creditable modeling and proper validation. Over the past decades both offline land model validations with field data, especially through offline model intercomparisons [Project for the Intercomparison of Land-Surface Parameterization Schemes (PILPS), Pitman and Henderson-Sellers 1998], and coupled atmosphere–land model intercomparison [Global Land–Atmosphere Coupling Experiment (GLACE), Koster et al. 2006] have been applied to several regions. PILPS is designed to improve the parameterization of the continental surface, especially hydrological, energy, momentum, and carbon exchanges with the atmosphere. GLACE focuses on a critical element of numerical weather and climate modeling: land–atmosphere coupling strength and the degree to which anomalies in land surface state (e.g., soil moisture) can affect rainfall generation and other atmospheric processes. These efforts have greatly improved land models and our understanding of VBPs and have laid the foundations for the present assessment of VBP effects on the global scale. This is addressed further in section 6.

The role of land surface processes in the climate system needs to be demonstrated for accurate climate simulation and prediction. The validation of VBP effects using

observational data presents another challenge. Without observational data as constraints, findings solely based on model results are hard to be used in a society's decision-making process. There have been only few direct, large-scale field studies of VBP–atmosphere relationships, and even fewer have intended to deduct relevant information from observational data to validate simulated vegetation–climate interactions. However, application of limited observation has been found to effectively highlight VBP effects in a few regional climate simulation studies (Beljaars et al. 1996; Zeng et al. 1999; Hong and Kalnay 2000; Douville et al. 2001; Xue et al. 2001, 2004b, 2006; Wang et al. 2004). In the present study we used observed global precipitation and surface temperature as references to diagnose the degree of VBP effects, since precipitation is a key component of the climate system and is particularly sensitive to those effects: the surface temperature is the result of the surface energy and water balances.

2. Models and experimental design

Two atmospheric general circulation models (AGCMs) were used in this study, both forced with prescribed sea surface temperature: the University of California, Los Angeles (UCLA) AGCM with horizontal resolution of 2° latitude by 2.5° longitude and 29 vertical levels (Mechoso et al. 2000) and the National Centers for Environmental Prediction (NCEP) AGCM (Kanamitsu et al. 2002a) with horizontal resolution T42 and 18 vertical levels. The UCLA AGCM and the NCEP AGCM have different physical parameterizations and numerical frameworks. Application of these two AGCMs provides an estimate of consistency and limited covalidation of results that can be model dependent.

The UCLA AGCM is a state-of-the-art gridpoint model of the global atmosphere extending from the earth's surface to the top of 1 hPa. The prognostic variables of this AGCM are the horizontal wind, potential temperature, water vapor mixing ratio, cloud liquid water and cloud ice water, planetary boundary layer (PBL) depth, surface pressure, and land surface temperature. Parameterization of the cumulus convection and its interaction with the PBL follows Pan and Randall (1998). The geographical distribution of sea surface temperature is prescribed based on a 31-yr (1960–90) climatology corresponding to the Global Sea Ice and Sea Surface Temperature (GISST) version 2.2 dataset (Rayner et al. 1995). More details on the UCLA AGCM can be found online at http://www.atmos.ucla.edu/_mechoso/esm. The NCEP AGCM that we used was a version of the NCEP seasonal forecast model (Kanamitsu et al. 2002b) placed on the Concurrent Versions System (CVS) server. This model has also been used for climate studies. This AGCM includes the Moorthi and Suarez (1992) convection scheme, Chou (1992) and Chou and Suarez (1994) radiation scheme, and Hong and Pan (1996) nonlocal planetary boundary layer scheme.

In both UCLA and NCEP AGCMs, the representations of VBP effects in the present study were provided by coupling to the Simplified Simple Biosphere Model (SSiB) (Xue et al. 1991, 1996). SSiB is a biophysically based model of land–atmosphere interactions intended for global and regional studies. In addition to interactive soil moisture and snow exchange, SSiB takes into consideration radiative transfer in the canopy and simulates diurnal and seasonal variations of albedo, canopy transpiration, and water interception loss. Furthermore, vegetation morphology and canopy resistance and their seasonal changes are taken into account in the computation of surface turbulent fluxes of water and sensible heat. Similarity theory was used to calculate the aerodynamic resistance from the canopy to the reference height. Based upon the Paulson (1970) and Businger et al. (1971) equations, a relationship between the Richardson number, vegetation properties, and aerodynamic resistance at the vegetated surface was developed and adjustments based on the vegetation conditions were introduced (Xue et al. 1991). In the SSiB the distribution of land cover properties was taken from a world vegetation map based on satellite observations (Hansen et al. 2000). SSiB has been extensively calibrated and validated using field data (i.e., Robock et al. 1995; Chen et al. 1997; Xue et al. 1996, 2003; Kahan et al. 2006) and has been tested in coupled climate models for several regions over the world (Xue et al. 2004b, 2006; Xue 2005). In addition, SSiB has participated in many offline land model intercomparisons (i.e., Shao and Henderson-Sellers 1996; Chen et al. 1997; Nijssen et al. 2003) and has been tested in a GCM model comparison study (Koster et al. 2006; Guo et al. 2006), which examined model atmosphere–soil moisture coupling strength. In this intercomparison, SSiB showed a medium coupling strength in reference to other models. When coupling SSiB with the UCLA and NCEP GCMs, no additional adjustment in the GCMs have been made beyond replacing the original land schemes and the land–atmosphere interface.

To test the VBP effects we compare the simulations including SSiB with others by the AGCMs coupled to simpler land models as well as with the observations. The choice of a control land model, with which to compare SSiB results, is also important: otherwise simulation differences with two models may just represent the deficiency in modeling physical processes by the control base land model. We selected control models that incorporate physical principles in representing specific

TABLE 1. Summary of major differences in three land schemes.

	Land schemes		
	UCLA simple scheme	NCEP two-layer soil model	SSiB
Surface albedo	Specified monthly mean albedo	Specified monthly mean albedo similar to SSiB monthly means	Two-stream method with diurnal variation
Surface roughness length	Specified monthly mean roughness length	Specified monthly mean roughness length similar to SSiB monthly means	Specified monthly mean values based on vegetation characteristics
Soil moisture	Specified monthly mean soil moisture	Interactive soil moisture	Interactive soil moisture
Surface aerodynamic resistance	One aerodynamic resistance based on Deardorff (1972)	One aerodynamic resistance based on Miyakoda and Sirutis (1986)	Three aerodynamic resistances with adjustment for vegetation conditions
Stomatal resistance	No	No	Yes
Snow process	Specified monthly mean albedo considering the climatological snow position	Albedo is adjusted when snow exists. Snow melting is based on surface energy balance.	Albedo and roughness length are adjusted when snow exists. Snow melting/refreezing is based on surface energy balance.
Vegetation parameters, such as fraction coverage, LAI, etc.	No	No	Yes

land surface processes and have been tested extensively and evaluated in AGCMs with reasonable, if not the ''best,'' precipitation results that this type of land processes can achieve.

The UCLA AGCM has a very basic land surface model, and has been used in numerous studies on climate variability and ocean–atmosphere interactions, including El Niño–Southern Oscillation and the Asian monsoon (i.e., Arakawa 2000; Yu and Mechoso 2001). The basic land model specifies monthly land surface characteristics, such as monthly mean surface albedo, roughness, and ground wetness (Suarez et al. 1983). Although most of today's GCMs have much more detailed land surface parameterizations, we selected this to show the maximal effects of VBP processes because of its clear physical representation. In this study, we also used the NCEP GCM with a land model (Pan and Mahrt 1987), which is a two-layer soil model that simulates ground soil moisture exchange based on prescribed monthly mean distribution of vegetation albedo and surface roughness (Dorman and Sellers 1989), both of which are similar to those produced by the AGCM coupled with SSiB. This land model will be hereafter referred as SOIL. The lowest atmospheric model layer is the surface layer, where the Monin–Obukhov similarity profile relationship is applied to obtain the surface stress and sensible and latent heat fluxes (Miyakoda and Sirutis 1986). No explicit biophysical processes are included in SOIL. Soil temperature and soil volumetric water content are computed in two layers at depths 0.1 and 1.0 m with an implicit time integration scheme (Pan and Mahrt 1987). The processes represented in SOIL have been considered by many meteorologists at one time as sufficient to represent the VBP in the climate system. SOIL has been used in the NCEP reanalyses I and II (Kalnay et al. 1996; Kanamitsu et al. 2002a) and produced among the best global historical climate estimations so far. The simulations by the UCLA AGCM coupled to SSiB and the basic land surface process representation will be referred to as LA-VBP and LA-NOVBP, respectively. The simulations by the NCEP AGCM coupled to SSiB and SOIL will be referred to as NC-VBP and NC-SOIL, respectively. The major differences between these three land schemes are listed in Table 1. All simulations correspond to five-member ensembles of one-year-long runs from five slightly different initial conditions obtained from the NCEP–National Center for Atmospheric Research (NCAR) global reanalysis (Kalnay et al. 1996). The UCLA GCM model ensemble was created through multiyear continuous simulations. Since the climatological SST is repeated every year and atmospheric and land surface conditions of different 1 Januarys are not identical to each other, each year represents a different member in an ensemble of one-year-long runs. The first year UCLA GCM run was not included in the five ensemble members. For this study the UCLA and NCEP AGCM were run for a total of 10 years each.

In the assessment, a key step is to determine whether differences in model outputs from with/without more comprehensive VBP representation are physically consistent with VBP effects in real world. Since a more realistic representation of VBPs in an AGCM should

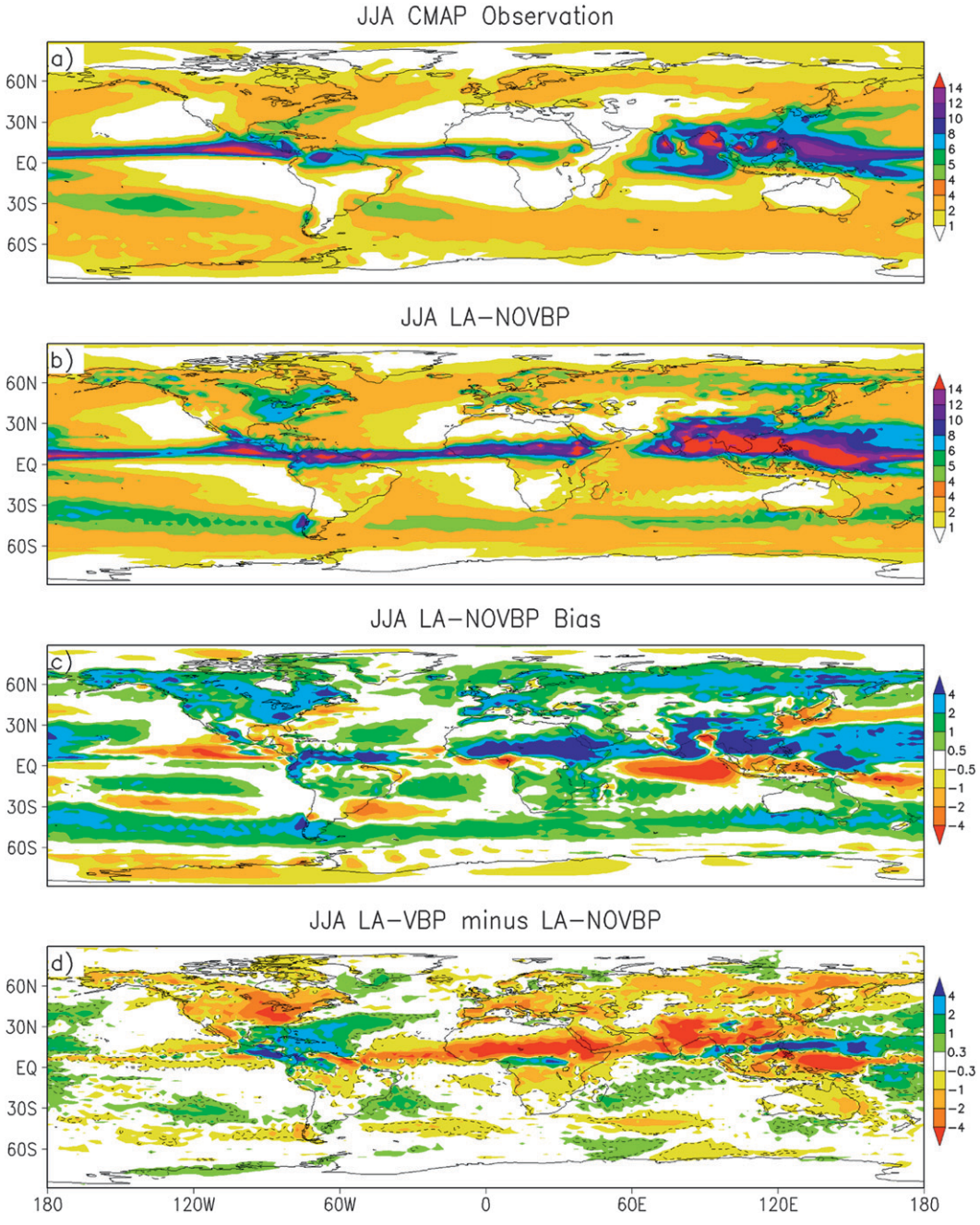

FIG. 1. Observed and simulated JJA precipitation (mm day^{-1}): (a) CMAP, (b) LA-NOVBP, (c) bias of LA-NOVBP, (d) LA-VBP minus LA-NOVBP. The dashed lines in the figures indicate values statistically significant at the 90% level in a two-tailed t test.

improve precipitation simulations if VBP has effects on the real climate system, we will adopt the statistically significant reduction of absolute bias and rms errors (RMSE) between simulated precipitation and the observation as criteria to identify VBP effects. Also, in our framework, the differences between NC-VBP and NC-SOIL are only partially due to VBP effects since SOIL already includes some of the effects represented in SSiB. We can reasonably expect the differences between these two simulations to be smaller than those between LA-VBP and LA-NOVBP if the climate system is sensitive to VBPs. Therefore, we analyzed whether precipitation errors are smaller in 1) the simulations coupled to SSiB than in those with simpler land models

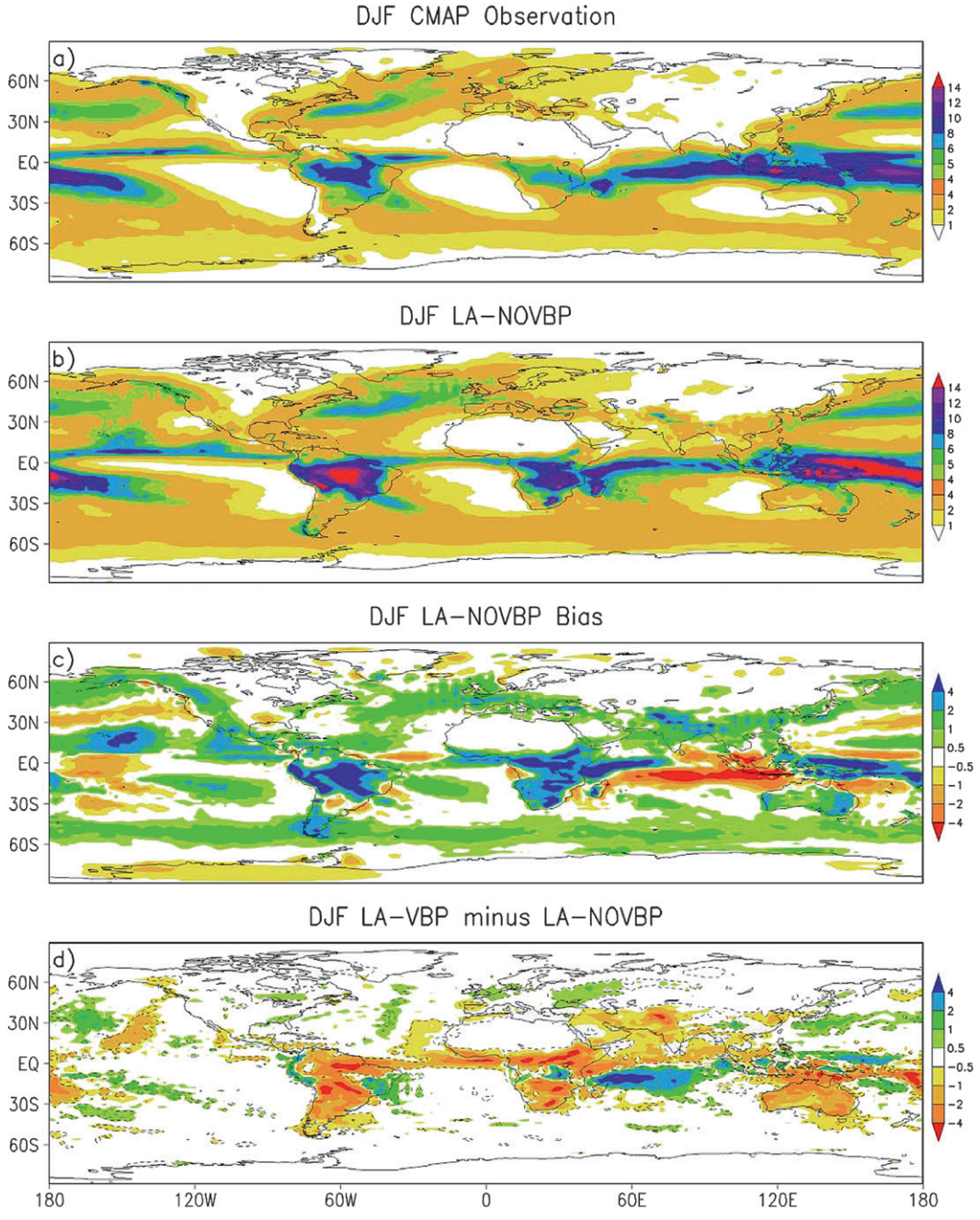

FIG. 2. As in Fig. 1 but for DJF precipitation.

and 2) the NCEP AGCM than in the UCLA AGCM simulations. The precipitation observations were from the Climate Prediction Center Merged Analysis of Precipitation (CMAP) (Xie and Arkin 1997).

The results from the two AGCMs should be consistent and the comparison between two AGCMs therefore provides a way for cross validation of the model results. If, in any region or season, the introduction of VBPs made the precipitation simulation results worse, that region or season was not further analyzed in this study since it is not clear whether the VBP model and/or AGCM have deficiencies in representing real VBP or VBP has no effect on this region/season. Conclusions in these cases are likely to be unreliable. Owing to the scope of this paper, we will not explore the possible cause(s) of model deficiencies in these regions.

TABLE 2a. Annual precipitation (mm day^{-1}) and differences of absolute bias and RMSE of simulations between LA-VBP and LA-NOVBP. The number in parentheses is relative difference.

Region	CMAP	LA-NOVBP	LA-VBP	Absolute bias difference	RMSE difference
Land	1.88	3.18	2.37	−0.81 (−62%)	−0.61 (−42%)
Ocean	3.00	3.37	3.32	−0.05	−0.05
Globe	2.67	3.32	3.05	−0.27 (−41%)	−0.19 (−18%)
Monsoon land	3.35	5.43	4.00	−1.41 (−72%)	−1.16 (−58%)
Midlatitude land	1.96	3.52	2.58	−0.87 (−58%)	−0.72 (−47%)
High-latitude land	1.16	2.24	1.83	−0.41 (−39%)	−0.41 (−38%)

3. VBP effects

Figures 1 and 2 show 5-yr averages of mean precipitation over the periods June–August (JJA) and December–February (DJF) from the CMAP observational dataset and LA-NOVBP, LA-VBP, the biases of LA-NOVBP, and differences between LA-VBP and LA-NOVBP. It is apparent that LA-NOVBP captured major features in the distribution of global precipitation in boreal and austral summers, especially the tropical convergence zones and their seasonal migrations, continental monsoon areas, the band of secondary maximum precipitation in midlatitudes, and dry regions along the west coasts of the continents (Figs. 1a,b and 2a,b). However, there were clear biases over most land areas, particularly over the monsoon regions (Figs. 1c and 2c). The bias in LA-NOVBP over land was 1.3 mm day^{-1}, or about 69% of the observed value; the corresponding numbers over the ocean were much less, 0.37 mm day^{-1} and 12% (Table 2a). Similar systematic errors have been reported in results obtained by an AGCM with a simple representation of land surface processes known as the ''bucket model'' (Sato et al. 1989). The differences between LA-VBP and LA-NOVBP were statistically significant differences in monsoon regions and large-scale continental areas (Figs. 1d and 2d). The dashed lines in the figures indicate values statistically significant at the 90% level in a two-tailed t test ($P < 0.000\,001$). The differences between LA-VBP and LA-NOVBP clearly show a reduction in precipitation biases due to VBP in most regions and seasons.

To further identify regions with strong VBP–atmosphere interactions, we examined the differences of absolute bias and RMSE between LA-VBP and LA-NOVBP globally and in three types of regions: 1) monsoon land, 2) midlatitude land, and 3) high-latitude land (Table 2b). We used absolute values since LA-VBP and LA-NOVBP could have different signs of biases. The geographic locations of the regions in Table 2b are listed in Table 3. The region labeled eastern Australia consists mainly of nonmonsoon areas because the Australian monsoon itself covers only a very limited land area with just a few AGCM grid cells. However, the temporal characteristics of VBP impacts in oceanic eastern Australia were quite consistent with those in other monsoon regions.

Table 2b indicates that VBPs have significant impacts on the water cycle over land. All difference values in Table 2b are negative, meaning that consideration of VBP reduced the bias/RMSE in all types of regions. VBPs in the GCM reduced the bias and RMSE in the LA-NOVBP simulation by 60% and 40% over land, respectively. The differences in bias and RMSE between VBP and NOVBP account for 43% and 33% of the observed precipitation over land, respectively. After carefully examination, we found only one major land region of the world with a larger bias in the annual

TABLE 2b. Differences of absolute bias and RMSE of annual mean precipitation (mm day^{-1}) between LA-VBP and LA-CNTL for subregions.

Category		Region	Absolute bias difference	RMSE difference
Monsoon land	1	West Africa	−2.01	−1.70
	2	East Asia	−1.54	−1.23
	3	South Asia	−1.50	−1.05
	4	Amazon	−1.33	−1.10
	5	Eastern Australia	−1.21	−0.97
	6	Central and East Africa	−1.18	−1.08
	7	Southeast Asia	−0.94	−0.48
	8	North American monsoon	−0.7	−0.69
Midlatitude land	1	Tibet Plateau	−1.19	−1.15
	2	Southern Africa	−1.0	−0.92
	3	South American savanna	−0.9	−0.24
	4	Northeast Asia	−0.88	−0.66
	5	Eastern United States	−0.77	−0.63
	6	Southern Europe	−0.76	−0.69
	7	Western United States	−0.67	−0.61
High-latitude land	1	Canada boreal	−0.40	−0.40
	2	Siberia	−0.41	−0.41

TABLE 3. Domain coordinates of subregions in Tables 2b, 4b, 5, and 6b.

Subregion	Coordinate			
Amazon	75°W	50°W	12°S	5°N
Canada boreal	125°W	60°W	50°N	65°N
Central and East Africa	10°E	45°E	10°S	5°N
East Asia	105°E	122°E	20°N	42°N
Eastern Australia	135°E	155°E	40°S	10°S
Eastern United States	100°W	65°W	30°N	45°N
North American monsoon	115°W	103°W	20°N	33°N
Northeast Asia	122°E	150°E	30°N	55°N
South American savanna	65°W	40°W	28°S	12°S
Siberia	60°E	180°	55°N	75°N
South Asia	60°E	92°E	10°N	20°N
Southeast Asia	92°E	110°E	5°S	20°N
Southern Africa	10°E	50°E	35°S	10°S
Southern Europe	10°W	60°E	35°N	55°N
Tibetan Plateau	80°E	105°E	28°N	37°N
West Africa	20°W	15°E	8°N	20°N
Western United States	120°W	100°W	30°N	45°N

precipitation in the LA-VBP simulation than with LA-NOVBP: the La Plata basin in South America. Following the rationale in the previous section, the VBP effects over this basin are not discussed further here.

Table 2b also indicates that the largest impacts of VBP were in the monsoon regions, where the average bias and RMSEs reductions were more than 1 mm day^{-1} and 10% higher than the mean reductions of global land. Among monsoon regions (Table 2b), the most affected was West Africa, consistent with many Sahel land–atmosphere interaction studies listed in the introduction. The weakest effects were in Southeast Asia and North America. The monsoons in the latter two regions develop over relatively narrow land areas surrounded by oceans and their circulations may be dominated by ocean conditions and complex ocean–land–atmosphere interactions, resulting in a weaker contribution of VBP effects than elsewhere.

In the midlatitude land, reduction in biases and RMSE varied less between subregions than in monsoon land. The regional average bias and RMSE reductions were close to the global land average (Table 2a). Overall, reductions in bias and RMSE due to VBP over the midlatitude regions were about 44% and 36% of the observed precipitation over the region, respectively. Table 2b shows that VBP effects have relative large impact over the Tibetan Plateau, where land–atmosphere interactions have not been emphasized so far. The reduction in RMSE for the South American savanna was substantially lower, probably caused by the same factors mentioned for the low impact on the North American monsoon. The VBP effects in high latitudes were significant and fairly homogeneous, but relatively weak, where the energy is relatively less and hydrological cycle weaker compared with low latitudes. On average the bias reduction over these regions was about 33% of the observed precipitation. The reductions in bias and RMSE in high latitudes were almost the same in two subregions, in contrast to monsoon regions where the reduction of RMSE and bias differ strongly, consistent with a more homogeneous spatial precipitation distribution and relative uniform land cover distribution in high latitudes.

The temporal characteristics of VBP effects are shown in Fig. 3, which presents the absolute bias reduction between LA-NOVBP and LA-VBP over different regions as a function of season. The reduction of RMSE had similar features (not shown). Impacts were large in most monsoon regions during seasons other than winter, that is, during the monsoon onset, mature, and withdraw stages. In summer, differences in bias in West Africa, East Asia, and the Amazon were larger than 2 mm day^{-1}. In spring, VBP effects resulted in bias reduction over all monsoon regions, particularly in East Asia, South Asia, and central and eastern Africa. The impact was also strong in the fall season for most regions, especially in West Africa, South Asia, and the Amazon, where it exceeded 2 mm day^{-1}. In winter, when precipitation is low and available energy is low, VBP impacts were generally weak.

In the midlatitude and high-latitude regions the strongest VBP impact was in spring and summer. The differences in bias were generally greater than 1 mm day^{-1} in midlatitudes and about 0.8 mm day^{-1} in high latitudes. Among midlatitude regions, the impact on the eastern United States was relatively strong with a bias reduction of more than 1.5 mm day^{-1} in both seasons. A few marginally positive values appear in Fig. 3. Especially, South Asian summer and North American fall had relatively large increased bias, about 0.6 mm day^{-1}, because of the inclusion of VBP. In addition, for the Southeast Asia subregion, although the summer bias reduction was quite substantial at 1.62 mm day^{-1} (Fig. 3), the RMSE increased by 0.42 mm day^{-1} (not shown). These results indicate that LA-VBP has difficulties in capturing the VBP effects in some seasons and regions.

4. Partial VBP effects

The partial VBP effects are indicated by comparison of the two runs with the NCEP AGCM. Since NC-SOIL included just a few VBP components, differences between NC-VBP and NC-SOIL can be attributed to partial VBP effects. NC-SOIL overestimated global mean precipitation over land by about 0.39 mm day^{-1}, or

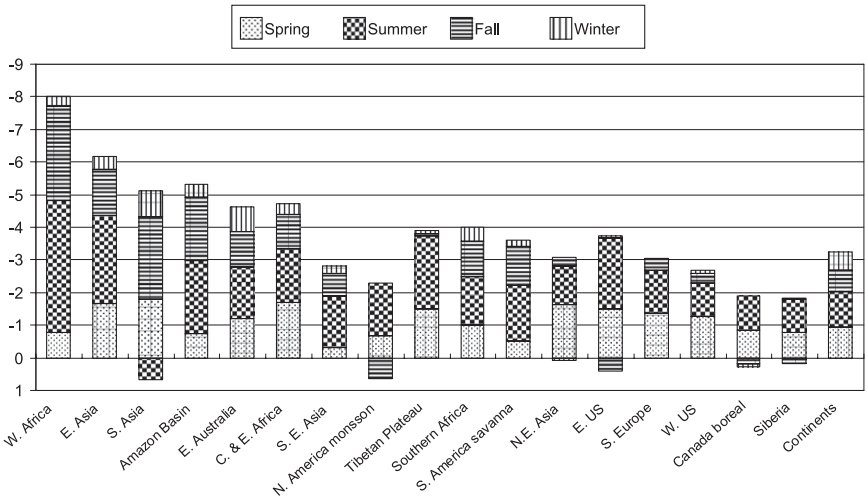

FIG. 3. Differences in absolute precipitation bias (mm day^{-1}) between the LA-VBP and LA-NOVBP over different regions in different seasons.

about 21% of the total precipitation over land (Table 4a). NC-VBP reduced the bias and RMSE over land by 0.24 mm day^{-1} and 0.14 mm day^{-1}, or about 13% or 8% of observed precipitation, respectively (Table 4a). The JJA and DJF results from these two simulations are shown in Fig. 4. Dashed lines in Figs. 4b,d indicate statistically significant values at the 90% level according to a two-tailed *t* test. The *P* values for the *t* test were smaller than 0.0002 for JJA and 0.025 for DJF. The largest differences again were over monsoon regions and large continents, albeit their geographic extent and magnitude were less than in the UCLA AGCM simulations, in which the full VBP effect was assessed.

In several regions with relative small land extent, mostly in the Southern Hemisphere (e.g., South Africa, eastern Australia, central and eastern Africa, and South American savanna), the differences between NC-VBP and NC-SOIL were small and without statistical significance (Figs. 4b,d). In eastern Australia, the annual mean precipitation bias in NC-SOIL was already very low: 0.07 mm day^{-1}. These results suggest that albedo, surface roughness, and interactive soil moisture, which are included in NC-SOIL, may be the dominant VBP components contributing to land–atmosphere interaction there. Alternatively, the AGCMs and/or SSiB may not adequately simulate the full VBP effect for some regions where NC-SOIL still produced substantial biases.

One interesting region is West Africa, which was most sensitive to VBP effects in summer according to the UCLA AGCM results. The NC-VBP also showed a summer bias reduction (0.38 mm day^{-1}), but it was not statistically significant (Fig. 4b). Other studies using this model (Xue et al. 2004b; Kang et al. 2007) with a higher resolution (T62, 28 levels) indicated that vegetation properties played a significant role in the seasonal and intraseasonal variations of precipitation over West Africa. The version used here had only few grid cells in the region, which may have contributed to the low statistical significance of the results. The situation was similar in the North American monsoon region where VBP effects resulted in substantial but nonsignificant bias reductions (Fig. 4b).

The results for regions other than those mentioned above indicate a consistent reduction of absolute bias of

TABLE 4a. Annual precipitation (mm day^{-1}) and differences of absolute bias and RMSE of simulations between NC-VBP and NC-SOIL. The number in parentheses is the relative difference.

Region	CMAP	NC-SOIL	NC-VBP	Absolute bias difference	RMSE difference
Land	1.86	2.25	2.01	−0.24 (−60%)	−0.14 (−15%)
Ocean	3.02	3.66	3.63	−0.03 (−1%)	−0.03 (−1%)
Globe	2.69	3.26	3.17	−0.09 (−16%)	−0.05 (−6%)
Monsoon	4.38	5.73	5.19	−0.55 (−46%)	−0.22 (−11%)
Midlatitude	1.69	2.29	1.82	−0.43 (−76%)	−0.29 (−38%)
High latitude	1.11	2.05	1.72	−0.33 (−36%)	−0.32 (−34%)

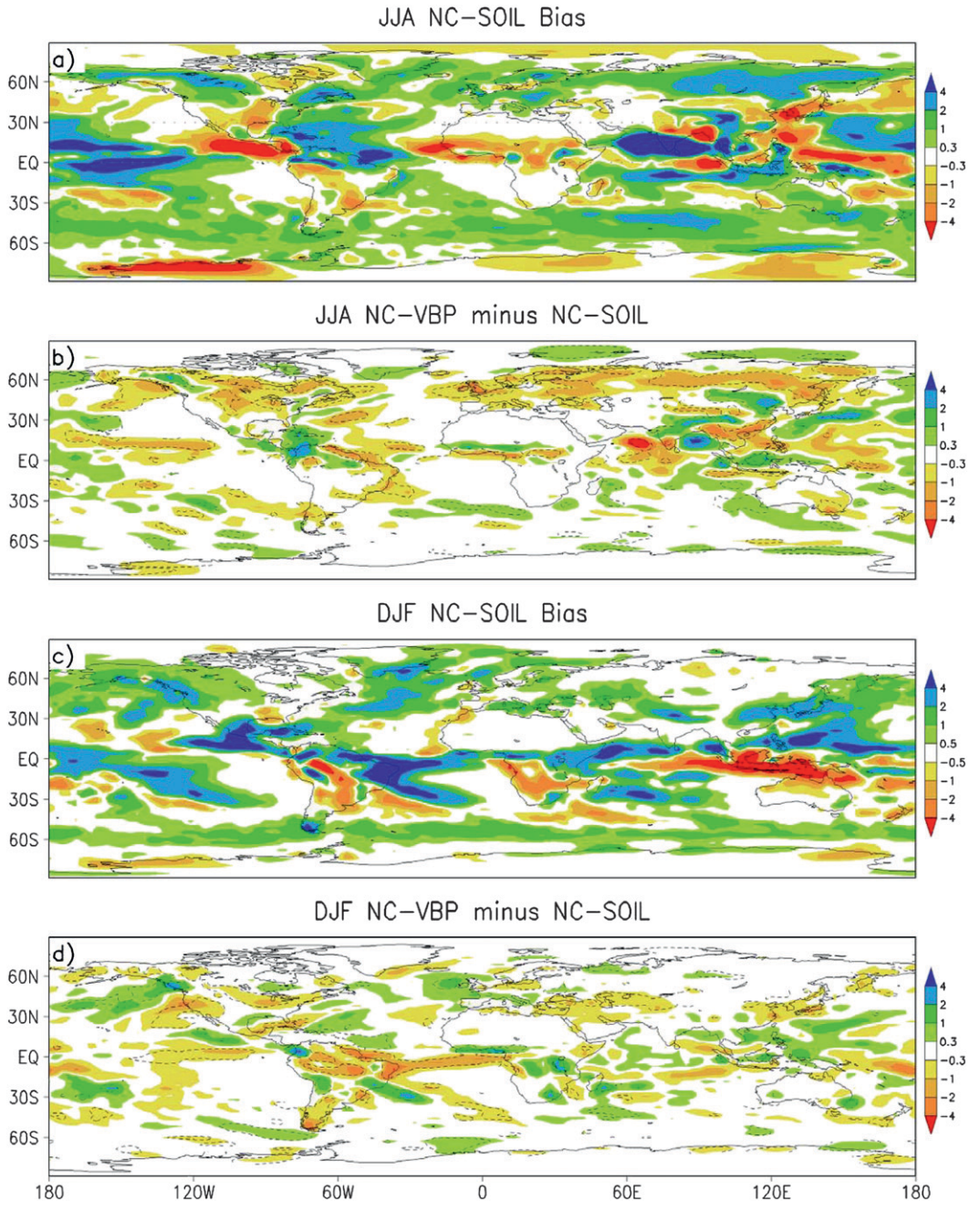

FIG. 4. Precipitation bias and simulation differences (mm day^{-1}): (a) NC-SOIL JJA simulation bias, (b) JJA simulation difference between NC-VBP and NC-SOIL, (c) NC-SOIL DJF simulation bias, and (d) DJF simulation difference between NC-VBP and NC-SOIL.

NC-VBP with respect to NC-SOIL (Table 4b), but less than those achieved with LA-VBP (Table 2b), as expected. Table 4b shows that the partial VBP effects were substantial in monsoon regions, midlatitude continental lands, and high-latitude lands. The bias differences due to partial VBP effects for these regions account for about 13%, 25%, and 30% of observed precipitation, respectively. Regional studies focused on the partial VBP effects have shown that the partial VBP effects on intraseasonal monsoon evolution over monsoon regions are strong (Xue et al. 2004b, 2006; Xue 2005).

In the northern high-latitude regions the bias and RMSE differences in Table 4a are very close (about 80%) to their differences in Table 2a, despite very different

TABLE 4b. Differences of absolute bias and RMSE of annual mean precipitation (mm day^{-1}) between NC-VBP and NC-SOIL for subregions.

Category		Region	Absolute bias difference	RMSE difference
Monsoon land	1	Amazon	−0.70	−0.23
	2	South Asia	−0.49	−0.50
	3	East Asia	−0.41	−0.12
	4	Southeast Asia	−0.39	−0.30
Midlatitude land	1	Northeast Asia	−0.58	−0.51
	2	Southern Europe	−0.42	−0.30
	3	Eastern United States	−0.38	−0.21
	4	Western United States	−0.37	−0.15
High-latitude land	1	Canada	−0.34	−0.30
	2	Siberia	−0.33	−0.33

AGCMs and experimental designs. The partial VBP effects, therefore, may account for a large portion of the VBP effect on this region. Since global warming is expected to have strong impacts on vegetation at northern high latitudes, this finding implies that a full assessment of future climate change in this region with AGCMs requires an adequate representation of VBPs.

In general, the UCLA AGCM and NCEP AGCM provided consistent results for the impacts of VBP on climate. Such is also the case in the La Plata basin, where the NC-VBP results were slightly worse than those of NC-SOIL, as with the LA-VBP and LA-NOVBP results. This suggests that SSiB may have difficulties in representing the region's VBPs and/or AGCMs' difficulties in capturing special features of this region's land–atmosphere system. The two AGCMs differed in one monsoon subregion, South Asia. Here, NC-VBP showed the larger impact, with a reduction of 0.7 mm day^{-1} in summer bias. The UCLA AGCM results were different in this regard, which indicated an uncertainty in estimation of VBP effects in the South Asian summer season with this model.

5. Water and energy budgets at the terrestrial surface

The simulated difference in precipitation obtained with different land processes was a result of changes in the surface energy and water balances. Land surface processes modulate the surface water and energy balances, which affect land–atmosphere interactions and the atmospheric circulations. In our previous summer regional land–atmosphere interaction study with the NCEP AGCM (Xue et al. 2004b, 2006; Xue 2005), it was found that the major simulation difference between the NCEP AGCM with/without explicit VBP was in surface heating, which modified the heating gradient between ocean and continent and, in turn, influenced pressure gradients, wind flow (through geostrophic balance in East Asia and ventilation in South America), and moisture transport. Evaporation and moisture flux convergence (MFC) played important roles for monsoon intraseasonal evolution in East Asia, the Sahel, and South America. In this paper, we mainly analyze the seasonal surface water and energy budgets in different runs to gain further understanding of their characteristics in land–atmosphere interactions. The surface water and energy budgets influence simulated changes in precipitation and circulation and were also affected by these changes. We will focus on the UCLA AGCM in this section since the NCEP AGCM produced consistent results, albeit with smaller magnitude in the seasonal means. In addition, the mechanisms of intraseasonal interaction in several regions have been comprehensively studied using the NCEP AGCM as discussed above.

The energy and water budget differences between LA-VBP and LA-NOVBP in summer are summarized in Table 5 (for summer only) and shown in Figs. 5–9. The summer season is JJA for the Northern Hemisphere and DJF for the Southern Hemisphere. Please note that differences listed in this table are actually not absolute differences as in previous sections. A striking feature in these figures was the difference in surface evaporation between the LA-VBP and LA-NOVBP over nondesert areas (Table 5 and Fig. 5). These differences were consistent with changes in precipitation and were the product of VBP at the surface and feedbacks from precipitation. LA-VBP consisted of stomatal resistance and three aerodynamic resistances, that is, aerodynamic resistance between canopy air space and atmosphere, aerodynamic resistance between surface soil layer and canopy height, and boundary layer resistance between canopy leaf surfaces and the canopy air space, while the LA-NOVBP has only one aerodynamic resistance connecting land and atmosphere without stomatal resistance. Higher surface resistance in the LA-VBP contributes to the simulated lower evaporation. In most regions in Table 5, the reductions of summer latent heat flux were larger than those in net radiation. Over the global land, the reduction in latent heat flux accounted for about 90% of the net radiation reduction.

Meanwhile, the evaporation difference between LA-VBP and LA-NOVBP exhibited clear spatial heterogeneity. There were only minor or negligible differences over desert areas. During boreal winter, most northern midlatitude and high-latitude lands had no difference

TABLE 5. Summer surface water and energy budgets differences between LA-VBP and LA-NOVBP. Variables are *P*: precipitation, *E*: evaporation, LH: latent heat flux, SH: sensible heat flux, Net Rad: net radiation, Net LW: net longwave radiation, and Net SW: net shortwave radiation; Units for *P* and *E* are mm day^{-1} and fluxes are W m^{-2}.

Region	*P*	*E*	*P* − *E*	LH	SH	Net Rad	Net LW	Net SW
West Africa	−4.05	−1.75	−2.30	−50.12	7.69	−43.28	−70.06	26.78
East Asia	−2.69	−1.52	−1.17	−43.20	18.08	−23.25	−40.45	17.19
South Asia	−3.86	−1.18	−2.68	−33.10	28.01	−14.33	−48.16	29.40
Amazon	−2.22	−0.55	−1.67	−14.92	11.79	−3.18	−19.73	16.55
Eastern Australia	−1.80	−3.13	1.33	−90.07	24.85	−65.23	−63.51	−1.71
Central and East Africa	−1.66	−1.60	−0.06	−45.50	14.59	−30.63	−37.03	6.4
Southeast Asia	−1.62	−0.45	−1.17	−12.05	−1.88	−14.33	−22.21	7.88
North American monsoon	−1.57	−2.13	0.56	−61.22	−8.33	−69.20	−58.15	−11.05
Tibet	−2.47	−1.69	−0.78	−48.15	11.39	−32.07	−44.4	12.33
Southern Africa	−1.49	−1.92	0.43	−54.73	11.23	−43.55	−41.9	−1.65
South American Savanna	−1.74	−2.31	0.57	−66.17	32.84	−33.71	−40.59	6.88
Northeast Asia	−1.72	−1.87	0.15	−53.47	27.86	−18.07	−39.81	21.73
Eastern United States	−3.13	−3.48	0.35	−99.95	45.55	−51.48	−57.59	6.11
Southern Europe	−1.31	−2.68	1.37	−77.11	15.78	−58.65	−58.35	−0.3
Western United States	−1.03	−2.28	1.25	−65.63	−12.39	−74.83	−56.95	−17.88
Canadian boreal	−1.07	−1.02	−0.05	−28.63	−1.16	−14.52	−26.59	12.08
Siberia	−1.04	−0.82	−0.22	−22.63	−14.86	−5.66	−22.88	17.22
Global land*	−0.81	−1.08	0.27	−30.48	−5.37	−34.15	−37.66	3.51

* Global land is based on annual mean.

and during austral winter, however, there were substantial differences over nondesert areas in the Southern Hemisphere. In addition, the difference over tropical rain forests—such as the Amazon, central Africa, and Southeast Asia—and over boreal forest areas was relatively small (Table 5, Fig. 5), less than about 1 mm day^{-1}. Forests typically have lower stomatal resistance and lower aerodynamic resistance compared with other vegetation types. Differences in evaporation rate were more than 2 mm day^{-1} in six regions (Table 5). Among them, five regions (eastern Australia, the North American monsoon region, the eastern and western United States, and southern Europe) had the largest changes in net radiation, which should contribute to the large reductions in evaporation there.

The net radiation consists of longwave and shortwave components. In the LA-VBP simulation, a lower evaporation rate led to higher surface temperature (to be discussed later) and less cloud cover (not shown). These conditions contributed to higher upward longwave radiation and lower downward longwave radiation, respectively, at the surface. The net longwave radiation decreased across continents (Fig. 6 and Table 5). The five regions mentioned above had the largest drop in net longwave radiation, 10–20 W m^{-2} higher than in other regions, contributing to the large overall reduction in net radiation. The semiarid West African region, in fact, also had the largest net longwave reduction (Table 5). However, the LA-NOVBP's evaporation in this semiarid region was not that high. The subsequent evaporation reduction in the LA-VBP was also less pronounced than in the five regions discussed above. Similar situations were found in desert areas where evaporation was either very low or negligible in LA-NOVBP. In addition to longwave radiation, net shortwave radiation at the surface, which was affected by surface albedo and cloud cover, also had an effect on the surface energy balance (Fig. 7). The lower amount of cloud cover allowed more downward shortwave radiation in LA-VBP. LA-VBP generally had higher surface albedo in the tropics and midlatitudes and lower albedo at high latitudes compared to LA-NOVBP (about 0.05–0.1, not shown), which produced high upward shortwave radiation over most land areas. However, the cloud effect dominated the net radiation change. The net shortwave radiation was increased over most areas. Among the areas listed in Table 5, net shortwave reduction only occurred in the North American monsoon area and the western United States, where the surface albedo increase was dominant in LA-VBP. The net shortwave radiation reduction in these two regions further contributed to the reduction in net radiation and then evaporation. Over most areas listed in Table 5, the change in net shortwave radiation was opposite to that in net longwave radiation (Table 5 and Figs. 6 and 7) but was generally much smaller. The net longwave change dominated the net radiation change at the surface (Table 5).

In addition to net radiation, the VBP also changes the partitioning between surface latent heat and sensible heat fluxes. Although evaporation over vegetated land generally decreased, the changes in sensible heat fluxes, however, were quite heterogeneous. In the areas listed

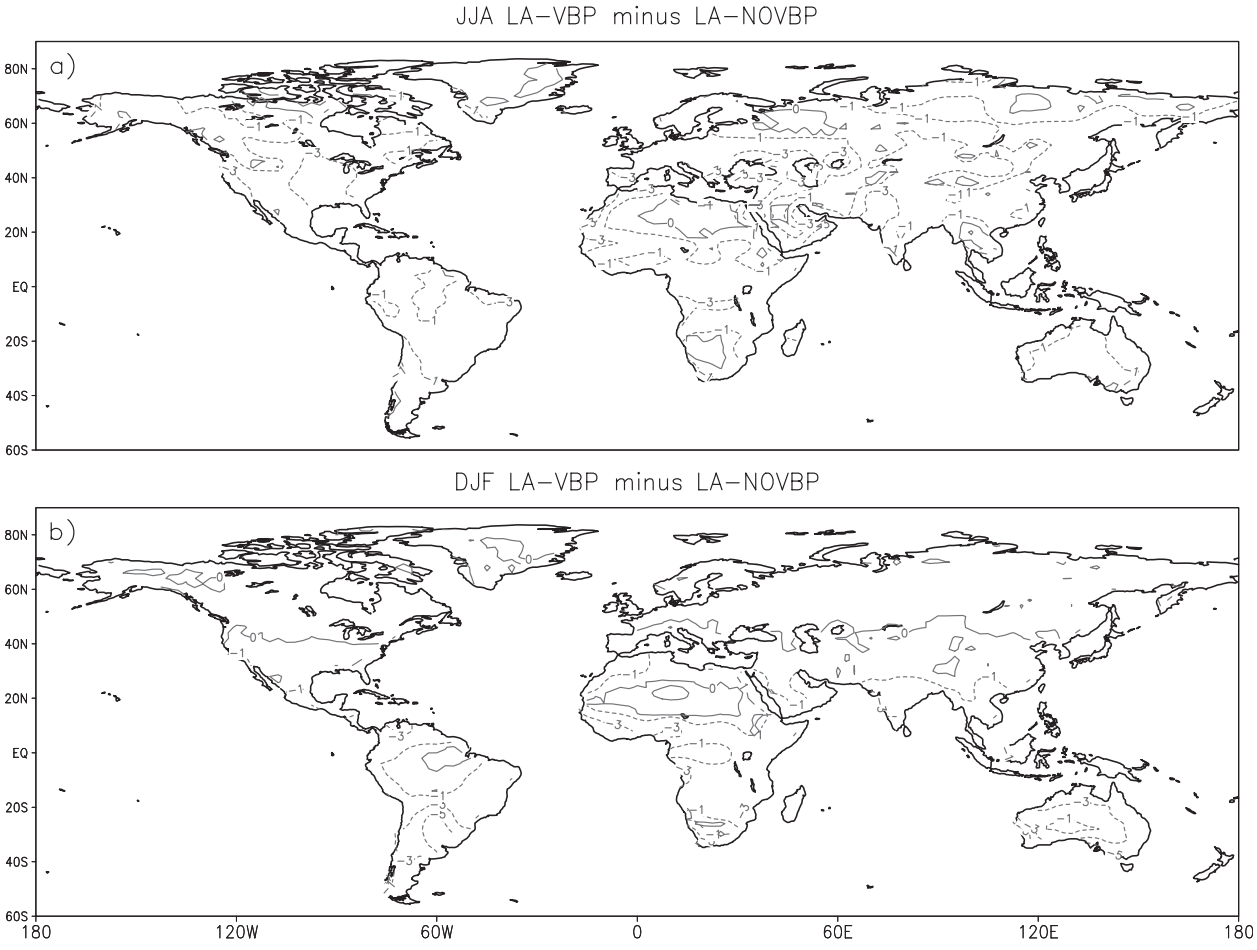

FIG. 5. Simulation differences of surface evaporation (mm day^{-1}) between the LA-VBP and LA-NOVBP for (a) JJA and (b) DJF, contours −5, −3, −1, and 0 mm day^{-1}.

in Table 5, where VBP had large evaporation reduction and showed strong impact on precipitation, the sensible heat flux was increased to balance the surface energy budget (Fig. 8 and Table 5). The areas with lower summer sensible heat flux in the LA-VBP included desert areas and some semiarid areas (Fig. 8), such as the western United States, where reduction in both latent heat flux and sensible heat flux balanced the reduction of net radiation. In the northern high latitudes, the LA-VBP produced high ground heat flux (not shown), which contributed to lower sensible heat flux there.

Changes in the heat gradient and moisture supply by the VBP modulated atmospheric circulation and precipitation. Changes in MFC, an important indicator of circulation and moisture transport, show distinct characteristics for the monsoon land, the midlatitude land, and the high-latitude land listed in Table 2b (Fig. 9). Over the monsoon regions, both MFC and surface evaporation in LA-VBP were reduced except in the eastern Australia and North American monsoon regions. Over the midlatitude lands, their changes had different signs; that is, evaporation was reduced but MFC was increased. Over the high latitudes, the MFC change was quite small (Table 5). Because a differential equation was used to calculate the MFC and this calculation was sensitive to temporal resolution, sample size, etc., and required high horizontal resolutions (Berbery and Rasmusson 1999), we used the difference between precipitation and evaporation in Table 5 to quantitatively represent MFC. Our previous land–atmosphere interaction studies over summer monsoon regions, such as the Sahel and East Asia, using the Center for Ocean–Land–Atmosphere Interaction Studies (COLA) AGCM (Xue 1996, 1997; Xue et al. 2004a) indicated that lower surface evaporation in JJA produced lower convective heating in the troposphere, followed by the production of relative subsidence, which in turn produced a reduction in convergence or an increase in low-level divergence. These effects seem consistent with the changes of evaporation and MFC in the monsoon land obtained in this

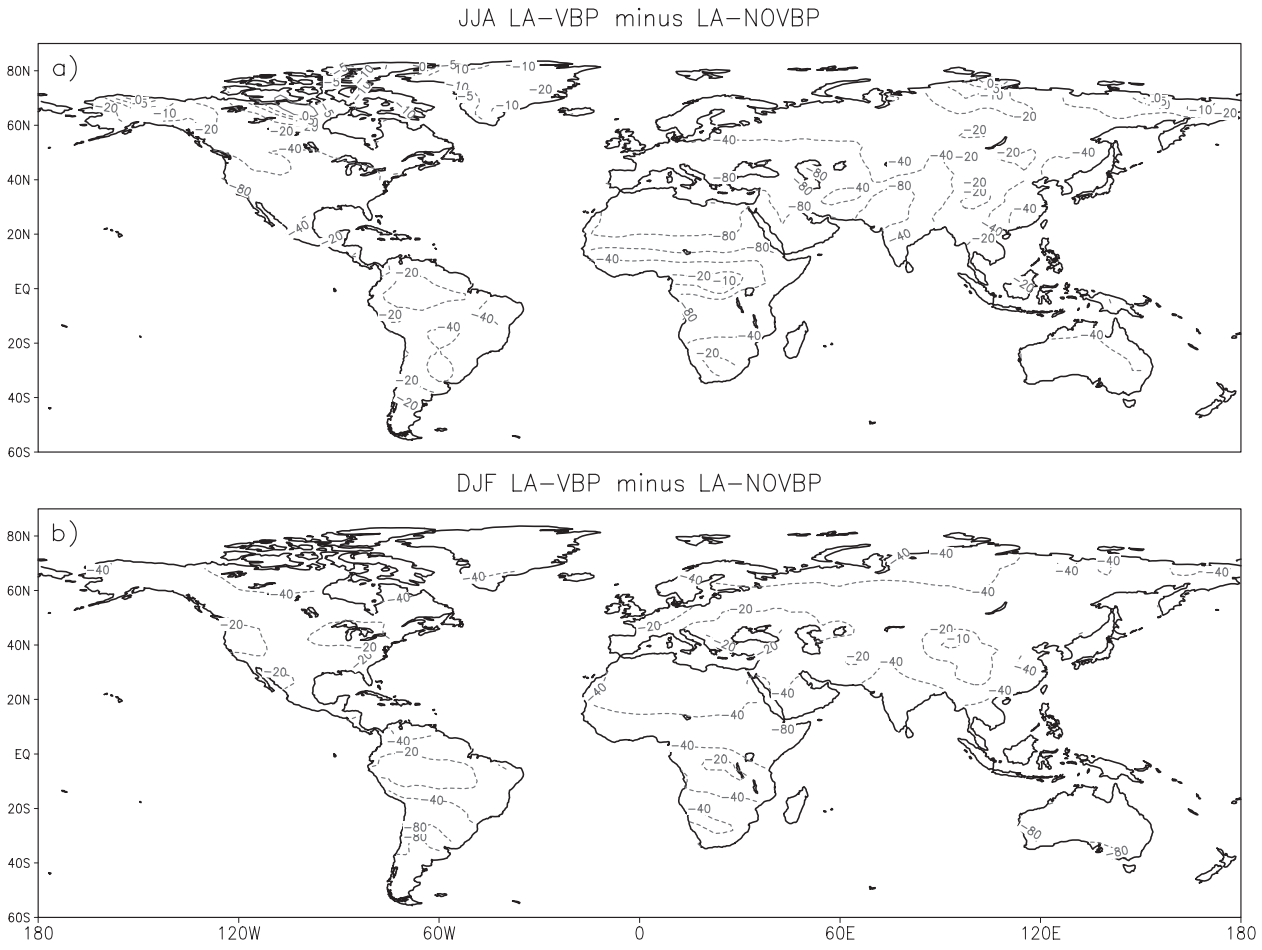

FIG. 6. As in Fig. 5 but for net longwave radiation (W m^{-2}) at the surface, contours −80, −40, −20, −10, −5, and 0 W m^{-2}.

study. On the other hand, the U.S. land–atmosphere interaction studies using the COLA AGCM and the regional Eta model (Xue et al. 1996, 2001) revealed that surface evaporation changes dominated the water cycle in land–atmosphere interactions in this region during the summer. When evaporation was lower, the convergence induced by the warm surface temperature (due to lower evaporation) normally partially compensated for the loss of moisture source by way of evaporation change, consistent with the changes in the midlatitude lands here.

There are a few exceptions in Table 5. For instance, MFC and evaporation changes had the same sign over the Tibetan Plateau as in the monsoon regions. The circulation over the Tibetan Plateau was strongly associated with others in South Asian and East Asian monsoons. It would not be surprising to find changes in MFC there consistent with the nearby monsoon regions (Fig. 9). In the North American monsoon and eastern Australian regions, the changes of MFC and evaporation had different signs, similar to the midlatitude regions. The difference between LA-VBP and LA-NOVBP shows very large scale convergence over the Gulf of Mexico (Fig. 9). The North American monsoon region only covers a narrow land area. Its circulation seems quite dominated by large-scale sea–land interactions. Another region, the eastern Australian, covers large midlatitude areas as indicated earlier. In the northern Australian monsoon region, however, both evaporation and MFC were reduced.

By and large, the land–atmosphere interactions are complex and nonlinear. How surface water and energy budgets affect circulation depends on land surface conditions, temporal and spatial scales, topographic features, and background climate conditions. Different geographic locations exhibit very different interaction characteristics and mechanisms. However, the monsoon regions, midlatitude lands, and high-latitude lands each exhibited quite different characteristics in circulation response to surface heating changes.

The changes in surface energy budget contributed to those in precipitation. Since there were no reliable

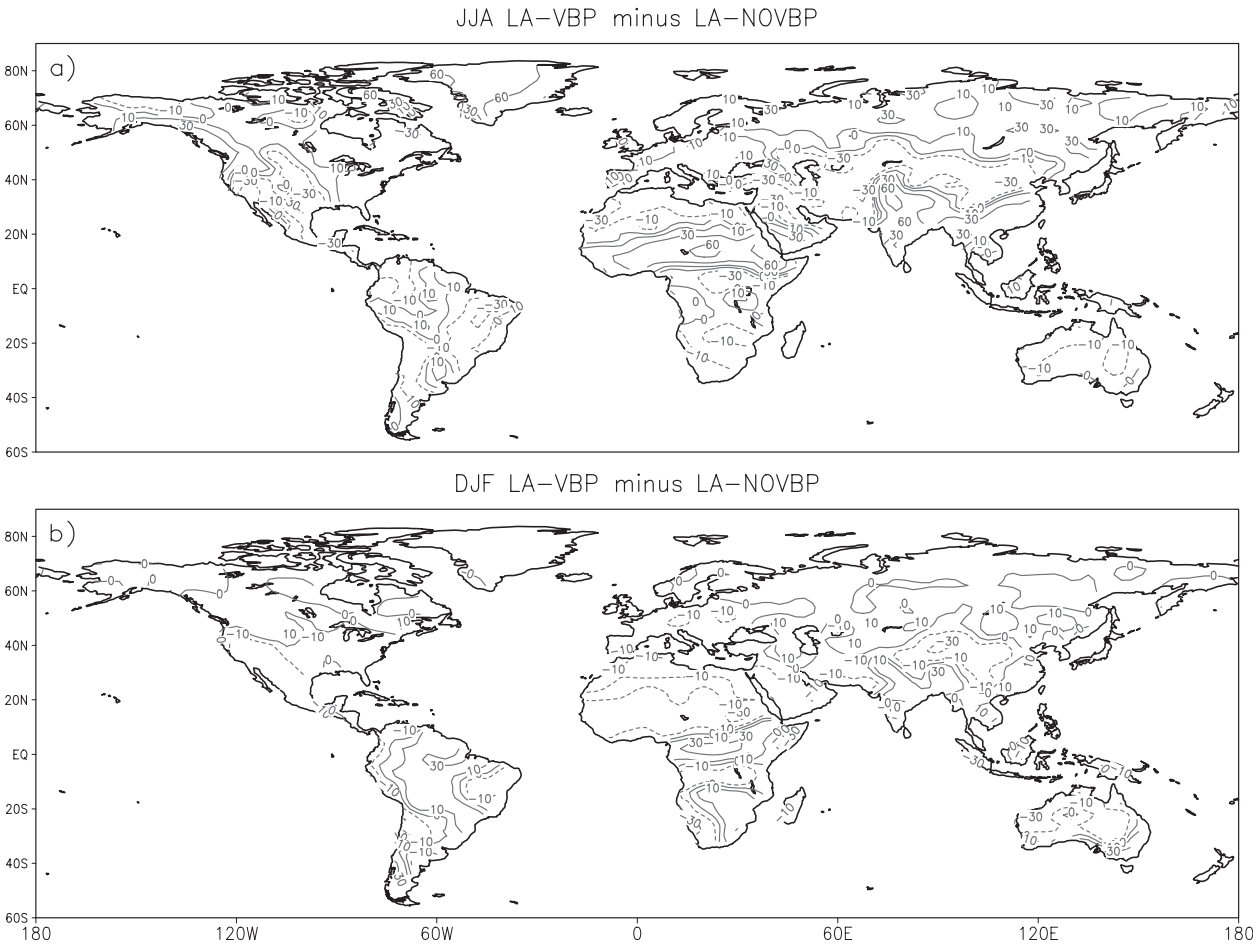

FIG. 7. As in Fig. 5 but for net shortwave radiation (W m^{-2}) at the surface, contours −30, −10, 0, 10, 30, and 60 W m^{-2}.

observational data to evaluate the LA-VBP surface energy and water budgets and because surface temperature is a product of the surface water and energy balances, we used surface temperature data from the Climate Anomaly Monitoring System station data archive (CAMS) to indirectly check the LA-VBP simulation of surface water and energy budget. The LA-NOVBP produced a cold bias in the Southern Hemisphere during JJA (Fig. 10) and a global cold bias, especially over the northern high latitudes, during DJF (Fig. 11). LA-VBP eliminated most cold biases during JJA but had a slightly warm bias over northern midlatitude lands. The warm bias over the Tibetan Plateau was quite large (Fig. 10). During DJF, LA-VBP eliminated most cold biases over the Southern Hemisphere and substantially reduced the cold bias over northern high latitudes (Fig. 11). Tables 6a,b shows that LA-VBP produced a global annual-mean surface temperature over land (excluding the Antarctic) very close to observations. Except for the Tibetan Plateau where observational sites were sparse and topography was complex, every other region in the table showed significant reduction in bias and RMSE. The substantial improvement in surface temperature simulation seems to support our notion that the simulated water and energy balance in the LA-VBP are reasonable.

6. Discussion and summary

When Sato et al. (1989) reported their results of one-month-long GCM simulations that demonstrated the advantages of using a biophysical model compared to a simple land model, there was speculation that application of simple adjustments (or tuning) of the simple land models may suffice to overcome the problems in the simulation without incorporating a parameterization of VBP processes. Since then, many studies have investigated this issue, including modifying the formulas and adjusting coefficients in the simple land scheme to reduce the evaporation rate. However, the comprehensive PILPS investigations (e.g., Shao and Henderson-Sellers

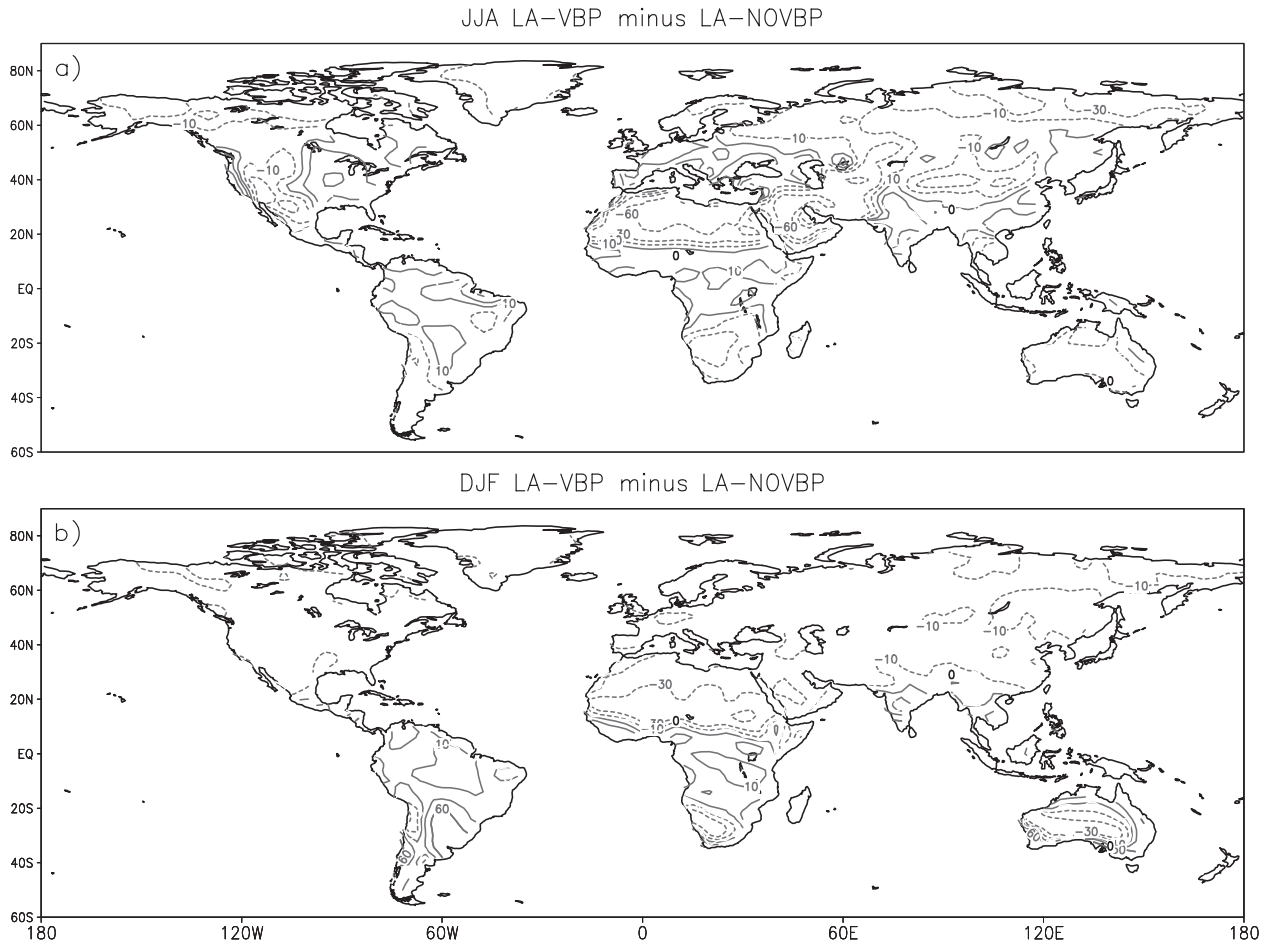

FIG. 8. As in Fig. 5 but for surface sensible heat flux (W m^{-2}), contours −60, −30, −10, 0, 10, 30, and 60 W m^{-2}.

1996; Chen et al. 1997) have clearly demonstrated that the simple land schemes by themselves (i.e., without VBP processes) have fundamental shortcomings and cannot produce the appropriate Bowen ratios. Pitman and Henderson-Sellers (1998), in summarizing the PILPS project achievements at that time, pointed out that, in the experiments conducted so far within PILPS, only the bucket (a type of simple land scheme) hydrology scheme has proven consistently anomalous compared with other land vegetation schemes. Because there is a consensus in the meteorological society today that the problems of simple land schemes cannot be fixed by parameter adjustments, every major GCM in the world has replaced the simple land scheme by a biophysical model, and we are able to use the simulation difference between these land schemes to assess the VBP effects.

The results obtained using two AGCMs coupled with different land surface schemes were largely consistent. The land schemes in this study are physically based process models, which have been extensively tested and comprehensively evaluated in numerous climate studies during the past two decades. By comparing results obtained by using SSiB and other land surface schemes representing different physical processes, this study provides a relatively objective and credible first global assessment of the regions and seasons in which VBPs exert strong effects.

A multimodel estimation (Koster et al. 2006) agreed that precipitation in three regions (Sahel, South Asia, and central United States) was affected by soil moisture anomalies during Northern Hemisphere summer. This agreement by no means suggests that these three are the only regions with strong summer land–atmosphere interactions. For example, a recent study (Seneviratne et al. 2006) has identified southern Europe as a region with strong soil moisture and atmosphere coupling. The present study also identifies southern Europe as a region with strong vegetation–atmosphere interaction in midlatitudes.

Our findings indicate that the VBP–atmosphere interactions, manifested here by their impact on precipitation, are primary components in the water cycle over

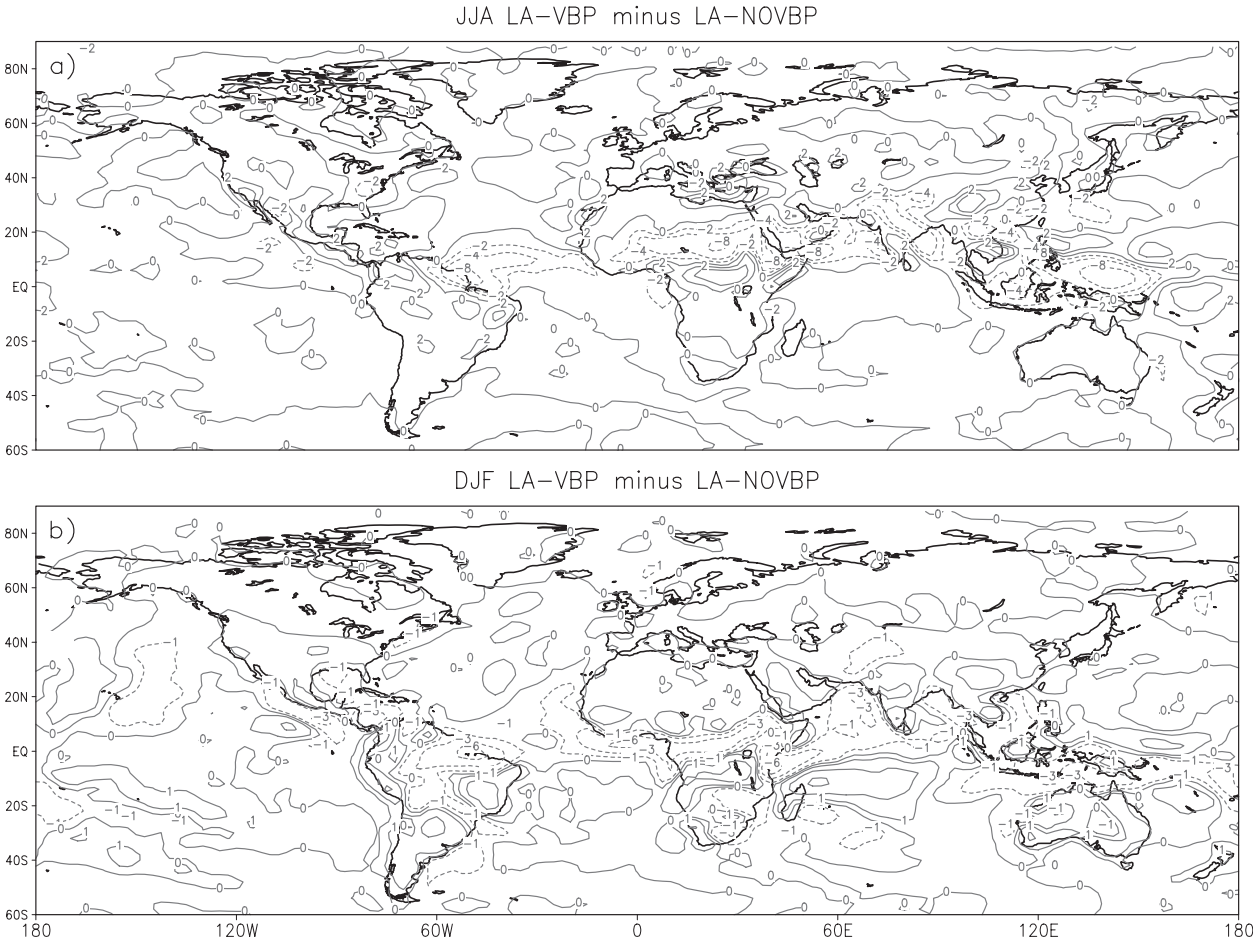

FIG. 9. As in Fig. 5 but for moisture flux convergence (mm day^{-1}), contours −8, −4, −2, 0, 2, and 4 mm day^{-1}.

land, with a particularly strong impact on monsoon regions. The simulated VBP effects on LA-VBP precipitation were estimated to be about 10% of observed precipitation globally and about 40% over land, while the partial VBP effects (excluding soil moisture and vegetation albedo) on NC-VBP annual precipitation over land were about 13%. Depending on regional climate characteristics and geographic conditions, the VBP impacts are strongest in spring, summer, and/or fall in different regions. The impact of VBPs in spring and fall was as strong as in summer in some regions, yet there are few studies of land–atmosphere interaction for these seasons. The results also detected significant partial VBP effects on the high northern latitudes. For the predominantly oceanic Southern Hemisphere, no significant differences were found between the full VBP and partial VBP effects. Studies using higher-resolution atmospheric models and better validated biophysical models over these regions are needed to further explore these issues in the Southern Hemisphere.

The analysis of surface energy and water budgets showed that the change in evaporation induced by VBPs was the dominant factor in modulating the surface energy and water balance. The VBP–cloud interaction had great influence on the net radiation at the surface, which was dominated by the net longwave change in the LA-VBP experiment. In the monsoon regions, the changes of surface evaporation and MFC were in phase, and both contributed to the atmospheric water cycle change. In mid and high latitudes, surface evaporation dominated the atmospheric water cycle in LA-VBP. This study was restricted to VBP impacts at continental and seasonal scales. The conclusions may be different in other spatial and temporal scales.

As indicated in the introduction, the early studies were mostly focused on the individual variables and processes (such as albedo, soil moisture, and surface roughness length). This study focuses on full VBP and partial VBP effects. In another study, Kang et al. (2007) found that using remote-sensing-derived global leaf area

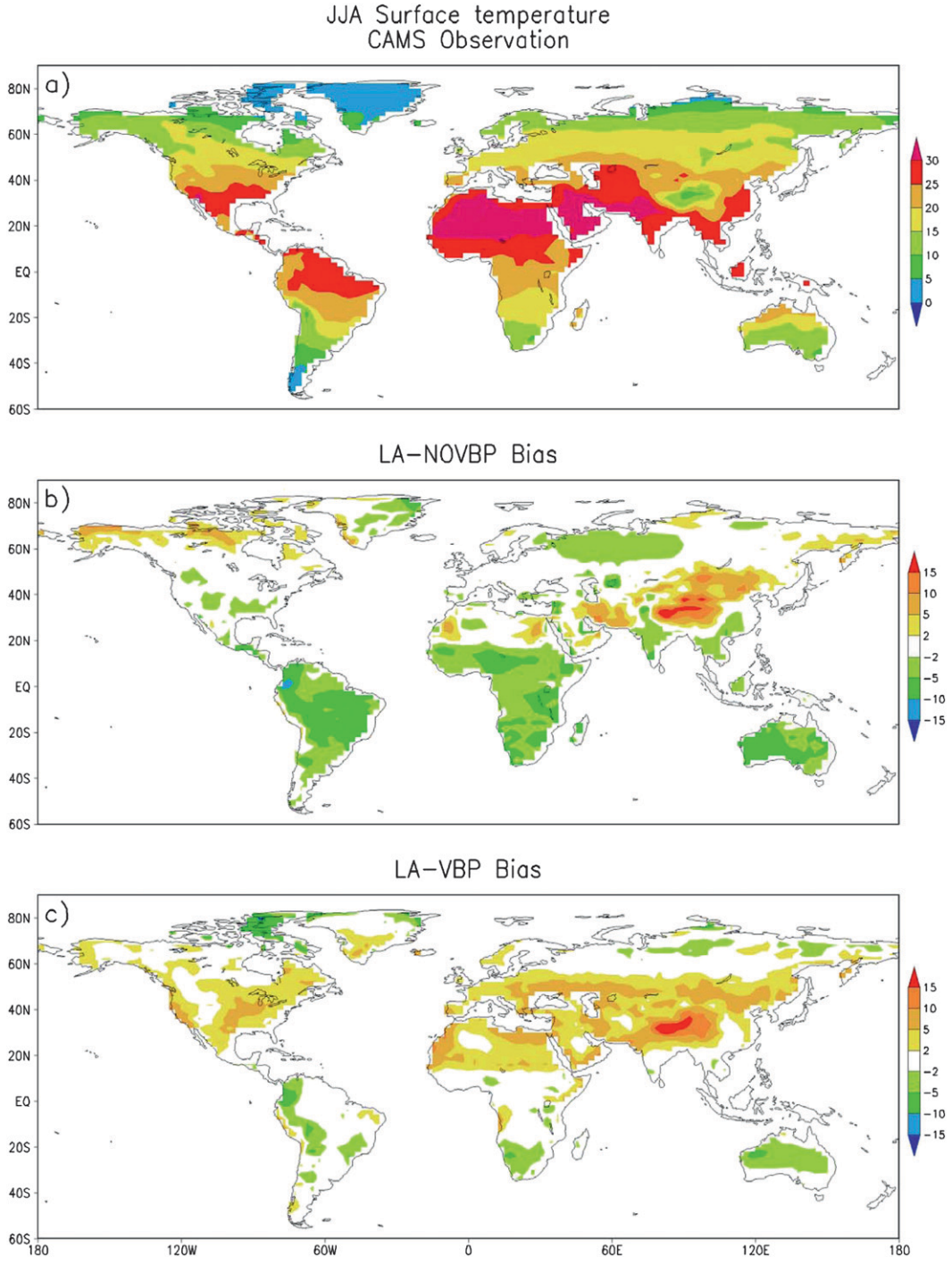

FIG. 10. Observed and the simulated JJA surface temperature (°C): (a) CMAP, (b) bias of LA-NOVBP, and (c) bias of LA-VBP.

index datasets, comparing with specified LAI based on a few ground surveys, the NCEP GCM produced substantial improvements in the near-surface climate in the summer monsoon areas of East Asia and West Africa and boreal forests of North America. However, they did not find significant differences over global land. Since the LAI is only a component of partial VBP, the results of Kang et al. (2007) are consistent with this study.

This is a modeling study and the results are model dependent; thus the conclusions should be regarded as

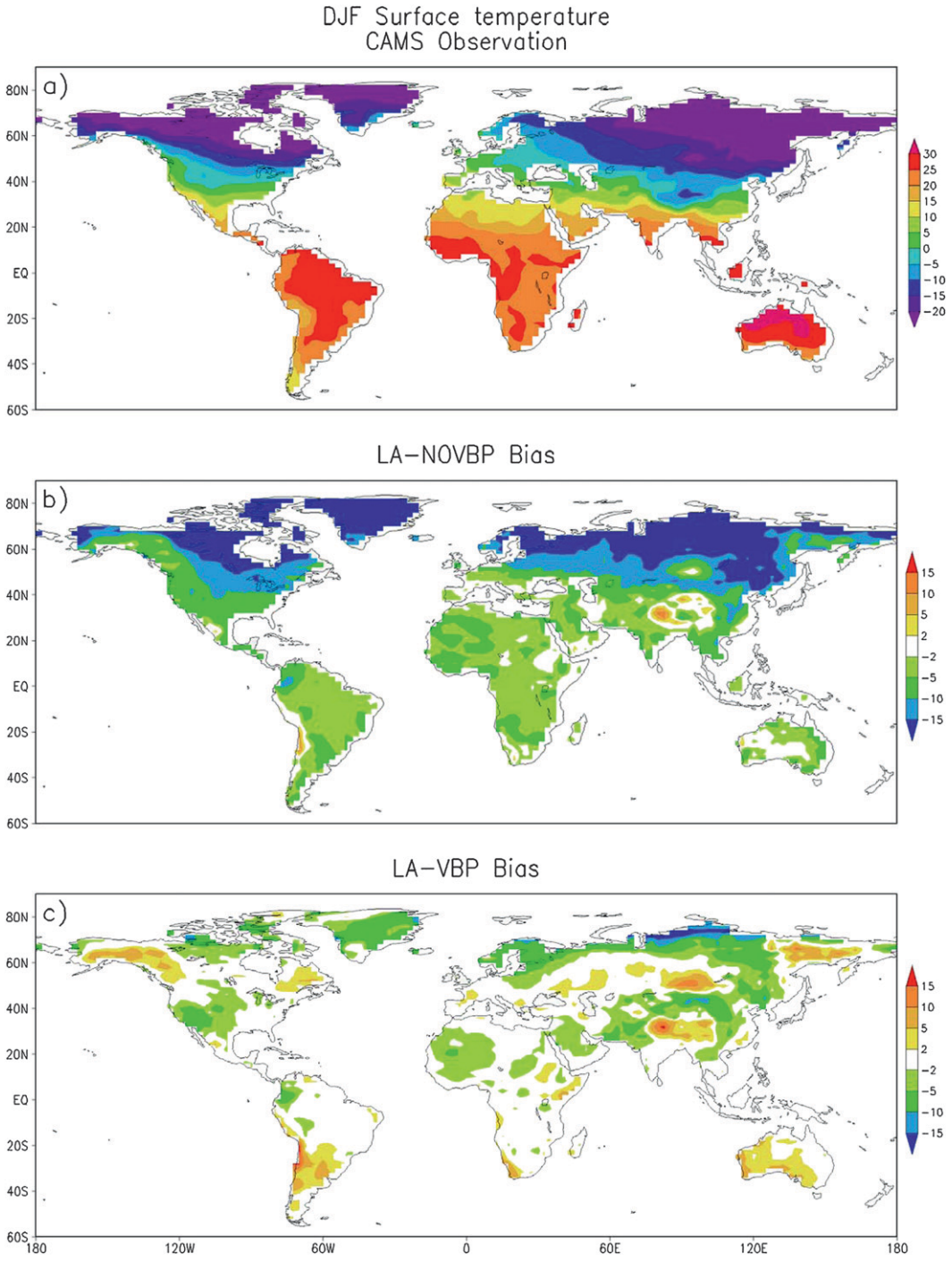

FIG. 11. As in Fig. 10 but for DJF.

preliminary. Furthermore, the potential effects of the initial soil moisture conditions that may affect the ground soil hydrology in the NCEP GCM were not investigated. Thus more modeling studies are necessary to evaluate the VBP impact. Recently efforts have been made to use satellite-derived products to assess VBP–atmosphere interactions (e.g., Liu et al. 2006; Los et al. 2006) and have opened a new approach to assessment of the VBP effects. With more observational data, such as those from satellite measurements, it has become possible to use actual measurements to validate and evaluate model findings in land–atmosphere interactions.

TABLE 6a. Annual surface temperature (°C) and differences in absolute bias and RMSE between LA-VBP and LA-NOVBP.

Region	CMAP	LA-NOVBP	LA-VBP	Absolute bias difference	RMSE difference
Land	13.99	9.56	14.22	−4.20	−2.38

Owing to caveats in satellite data acquisition and data processing, cross validation from both modeling and data diagnostic studies is necessary and can be expected to provide a more comprehensive understanding of land–atmosphere interactions. We hope our preliminary findings in this study will stimulate more studies to extensively and comprehensively understand the VBP feedbacks at different scales over different regions and with different land components.

Nevertheless, it is clear that representing this feedback in global climate change studies is critically important for climate system modeling and climate prediction. In our case, a comprehensive VBP representation in the UCLA AGCM could reduce the bias and RMSE in precipitation estimations over land by about 60% and 40%, respectively—a very substantial improvement. A direct benefit of improved simulation of VBP effects, therefore, should include improved present and future seasonal precipitation prediction. The inadequate representation of VBP effects in climate models can contribute greatly to uncertainty in climate change studies and future climate projections.

A recent climate model assessment concludes ''climate model simulation of precipitation has improved over time but is still problematic'' (Bader et al. 2008). This study shows that, with different representations of land surface processes, the difference in simulation of global and regional precipitation could be very substantial and produce large uncertainties in precipitation. Furthermore, a recent GLACE study (Koster et al. 2006) demonstrates that coupling between different GCMs and current state-of-the art land models can greatly vary in strength, also contributing to large uncertainty in climate simulation. All these works indicate the uncertainty and errors in VBP modeling are major sources contributing to uncertainty in current climate modeling.

Furthermore, although our study has focused on natural VBP effects on climate, since the physical processes to modulate the land role on the climate system and to determine the potential impact of anthropogenic climate change on vegetation and the hydrological cycle are the same (Dickinson 1992), the present findings are highly relevant to current climate change studies. Many policy decisions concerning mitigation of human impacts on climate through changes in emissions of greenhouse gases and land cover and land use changes are being based on coupled atmosphere–land surface models that may lack adequate treatment of vegetation–biosphere processes. This study suggests that the assessments of anthropogenic effects based on the three land models in this investigation would provide very different information.

Our emphasis has been mainly on land regions. Over the global ocean, neither the LA-VBP nor the NC-VBP show substantial impacts (Tables 2 and 4). Nevertheless, both simulations indicate impacts on several ocean areas

TABLE 6b. Annual mean surface temperature (°C) bias for LA-VBP and the difference in absolute bias and RMSE between LA-VBP and LA-CNTL for subregions (number).

Category		Region	LA-VBP bias	Absolute bias difference	RMSE difference
Monsoon land	1	West Africa	0.07	−4.53	−2.79
	2	East Asia	0.23	−3.03	−1.77
	3	South Asia	−0.33	−4.30	−3.19
	4	Amazon	−1.39	−2.93	−2.81
	5	Eastern Australia	0.48	−3.83	−2.66
	6	Central and East Africa	0.29	−3.47	−2.09
	7	Southeast Asia	−1.37	−4.30	−3.73
	8	North American monsoon	0.76	−1.91	−1.11
Midlatitude land	1	Tibetan Plateau	4.47	2.73	0.19
	2	Southern Africa	−0.26	−4.17	−2.76
	3	South American savanna	−0.47	−4.73	−3.64
	4	Northeast Asia	0.02	−4.82	−1.93
	5	Eastern United States	1.45	−3.15	−2.21
	6	Southern Europe	2.27	−0.62	−0.44
	7	Western United States	−0.59	−4.41	−2.37
High-latitude land	1	Canada boreal	0.16	−6.07	−4.11
	2	Siberia	−2.90	−6.62	−4.89

near monsoon regions with improvements in simulations. These areas include the Gulf of Mexico, eastern Pacific near Central America, parts of the southern Atlantic, Arabian Sea, Bay of Bengal, and parts of the western Pacific (Figs. 1d, 2d, and 4b,d). Since the SST was prescribed in this study, land–ocean–atmosphere interactions were suppressed. A fully coupled land–ocean–atmosphere model with multiyear simulations is necessary to comprehensively expand our findings.

This study suggests that it is important to apply observational data to assess VBP impact and to improve modeling ability to model VBP–climate interaction in different regions since VBP feedback is a complex process with substantially different regional signatures. Thus far, most land model validations, such as PILPS, focused the regions in Northern Hemisphere (the Amazon is probably the only exception). For the La Plata basin, where the AGCMs have difficulty to identify the VBP effect, SSiB has not been validated with in situ data. Today, when more observational data—especially the data from satellite measurements and from the Global Energy and Water Cycle Experiment (GEWEX) Coordinated Energy and Water Cycle Observation Project (CEOP)—are available, it is necessary to apply measurement data to validate and improve the vegetation model to produce realistic VBP effects for every major climate region. A realistic VBP representation should help reduce uncertainty in current climate models and produce reasonable climate simulations and projections.

Acknowledgments. This research was supported by NOAA Grants NA05OAR4310010 and NA07OAR4310226 and by the U.S. National Science Foundation Grants ATM-0751030 and NSF-ATM-0353606.

REFERENCES

Arakawa, A., 2000: A personal perspective on the early years of general circulation modeling at UCLA. *General Circulation Model Development: Past, Present, and Future—Proceedings of a Symposium in Honor of Professor Akio Arakawa,* D. A. Randall, Ed., Elsevier, 1–65.

Avissar, R., and D. Werth, 2005: Global hydroclimatological teleconnections resulting from tropical deforestation. *J. Hydrometeor.,* **6,** 134–145.

Bader, D. C., C. Covey, W. J. Gutowski Jr., I. M. Held, K. E. Kunkel, R. L. Miller, R. T. Tokmakian, and M. H. Zhang, 2008: Climate models: An assessment of strengths and limitations. U.S. Climate Change Science Program and the Subcommittee on Global Change Research, Department of Energy, Office of Biological and Environmental Research, 124 pp.

Bates, B. C., Z. W. Kundzewicz, S. Wu, and J. P. Palutikof, Eds., 2008: Climate change and water. Intergovernmental Panel on Climate Change Tech. Paper VI, 210 pp.

Beljaars, A. C. M., P. Viterbo, and M. J. Miller, 1996: The anomalous rainfall over the United States during July 1993: Sensitivity to land surface parameterization and soil moisture anomalies. *Mon. Wea. Rev.,* **124,** 362–383.

Berbery, E. H., and E. M. Rasmusson, 1999: Mississippi moisture budgets on regional scale. *Mon. Wea. Rev.,* **127,** 2654–2673.

Bonan, G. B., 2008: Forests and climate change: Forcings, feedbacks, and the climate benefits of forests. *Science,* **320,** 1444–1449.

——, D. Pollard, and S. L. Thompson, 1992: Effects of boreal forest vegetation on global climate. *Nature,* **359,** 716–718.

Businger, J. A., J. C. Wyngaard, Y. Izumi, and E. G. Bradley, 1971: Flux-profile relationships in the atmospheric surface layer. *J. Atmos. Sci.,* **28,** 181–189.

Charney, J., W. J. Quirk, S.-H. Chow, and J. Kornfield, 1977: A comparative study of the effects of albedo change on drought in semi-arid regions. *J. Atmos. Sci.,* **34,** 1366–1385.

Chase, T. N., R. Pielke, T. Kittel, R. Nemani, and S. Running, 1996: Sensitivity of a general circulation model to global changes in leaf area index. *J. Geophys. Res.,* **101,** 7393–7408.

Chen, T. H., and Coauthors, 1997: Cabauw experimental results from the Project for Intercomparison of Land-Surface Parameterization Schemes. *J. Climate,* **10,** 1194–1215.

Chou, M.-D., 1992: A solar radiation model for use in climate studies. *J. Atmos. Sci.,* **49,** 762–772.

——, and M. J. Suarez, 1994: An efficient thermal infrared radiation parameterization for use in general circulation models. NASA Tech. Rep. TM-1994-104606, Series on Global Modeling and Data Assimilation, 85 pp.

Claussen, M., 1997: Modeling bio-geophysical feedback in the African and Indian monsoon region. *Climate Dyn.,* **13,** 247–257.

Cox, P. M., R. A. Betts, C. D. Jones, S. A. Spall, and I. J. Totterdell, 2000: Acceleration of global warming due to carbon-cycle feedbacks in a coupled climate model. *Nature,* **408,** 184–187.

Deardorff, J. W., 1972: Parameterization of the planetary boundary layer for use in general circulation models. *Mon. Wea. Rev.,* **100,** 93–106.

Dickinson, R. E., 1992: Land surface. *Climate System Modeling,* K. E. Trenberth, Ed., Cambridge University Press, 689–701.

——, and A. Henderson-Sellers, 1988: Modelling tropical deforestation: A study of GCM land-surface parameterizations. *Quart. J. Roy. Meteor. Soc.,* **114,** 439–462.

Dirmeyer, P. A., and J. Shukla, 1994: Albedo as a modulator of climate response to tropical deforestation. *J. Geophys. Res.,* **99,** 20 863–20 877.

Dorman, J. L., and P. J. Sellers, 1989: A global climatology of albedo, roughness length and stomatal resistance for atmospheric general circulation model (SiB). *J. Appl. Meteor.,* **28,** 833–855.

Douville, H., F. Chauvin, and H. Broqua, 2001: Influence of soil moisture on the Asian and African monsoons. Part I: Mean monsoon and daily precipitation. *J. Climate,* **14,** 2381–2403.

Fu, C., T. Yasunari, and S. Lütkemeier, 2004: Asian monsoon climate. *Vegetation, Water, Humans and the Climate,* P. Kabat et al., Eds., Springer-Verlag, 115–127.

Guo, Z., and Coauthors, 2006: GLACE: The Global Land–Atmosphere Coupling Experiment. Part II: Analysis. *J. Hydrometeor.,* **7,** 611–625.

Hansen, M. C., R. S. DeFries, J. R. Townshend, and R. Sohlberg, 2000: Global land cover classification at 1 km spatial resolution using a classification tree approach. *Int. J. Remote Sens.,* **21,** 1303–1330.

Hong, S.-Y., and H.-L. Pan, 1996: Nonlocal boundary layer vertical diffusion in a medium-range forecast model. *Mon. Wea. Rev.,* **124,** 2322–2339.

——, and E. Kalnay, 2000: Role of sea surface temperature and soil-moisture feedback in the 1998 Oklahoma-Texas drought. *Nature,* **408,** 824–844.

Kahan, D., Y. Xue, and S. Allen, 2006: The impact of vegetation/soil parameters in simulations of surface energy and water balance in the semi-arid Sahel area: A case study using SEBEX and HAPEX-Sahel data. *J. Hydrol.,* **320,** 238–259.

Kalnay, E., and Coauthors, 1996: The NCEP/NCAR 40-Year Reanalysis Project. *Bull. Amer. Meteor. Soc.,* **77,** 437–471.

Kanamitsu, M., W. Ebisuzaki, J. Woollen, S.-K. Yang, J. J. Hnilo, M. Fiorino, and G. L. Potter, 2002a: NCEP–DOE AMIP-II Reanalysis (R-2). *Bull. Amer. Meteor. Soc.,* **83,** 1631–1643.

——, and Coauthors, 2002b: NCEP dynamical seasonal forecasting system 2000. *Bull. Amer. Meteor. Soc.,* **83,** 1019–1037.

Kang, H.-S., Y. Xue, and G. J. Collatz, 2007: Assessment of satellite-derived leaf area index datasets using a general circulation model: Seasonal variability. *J. Climate,* **20,** 993–1015.

Kleidon, A., K. Fraedrich, and M. Heimann, 2000: A green planet versus a desert world: Estimating the maximum effect of vegetation on the land surface climate. *Climatic Change,* **44,** 471–493.

Koster, R. D., and Coauthors, 2006: GLACE: The Global Land–Atmosphere Coupling Experiment. Part I: Overview. *J. Hydrometeor.,* **7,** 590–610.

Liu, Z., M. Notaro, J. Kutzbach, and N. Liu, 2006: Assessing global vegetation–climate feedbacks from observations. *J. Climate,* **19,** 787–814.

Los, S. O., G. P. Weedon, P. R. J. North, J. D. Kaduk, C. M. Taylor, and P. M. Cox, 2006: An observation-based estimate of the strength of rainfall-vegetation interactions in the Sahel. *Geophys. Res. Lett.,* **33,** L16402, doi:10.1029/2006GL027065.

Mechoso, C. R., J.-Y. Yu, and A. Arakawa, 2000: A coupled GCM pilgrimage: From climate catastrophe to ENSO simulations. *General Circulation Model Development: Past, Present and Future: Proceedings of a Symposium in Honor of Professor Akio Arakawa,* D. A. Randall, Ed., Academic Press, 539–575.

Miyakoda, K., and J. Sirutis, 1986: Manual of the E-physics, 122 pp. [Available from Geophysical Fluid Dynamics Laboratory, Princeton University, P.O. Box 308, Princeton, NJ 08542.]

Moorthi, S., and M. J. Suarez, 1992: Relaxed Arakawa–Schubert: A parameterization of moist convection for general circulation models. *Mon. Wea. Rev.,* **120,** 978–1002.

Nijssen, B., and Coauthors, 2003: Simulation of high-latitude hydrological processes in the Torne–Kalix basin: PILPS Phase 2(e): 2: Comparison of model results with observations. *Global Planet. Change,* **38,** 31–53.

Nobre, C. A., J. Shukla, and P. Sellars, 1991: Amazonian deforestation and regional climate change. *J. Climate,* **4,** 957–988.

Notaro, M., Z. Liu, R. Gallimore, S. J. Vavrus, J. E. Kutzbach, I. C. Prentice, and R. L. Jacob, 2005: Simulated and observed preindustrial to modern vegetation and climate changes. *J. Climate,* **18,** 3650–3671.

Pan, D.-M., and D. A. Randall, 1998: A cumulus parameterization with a prognostic closure. *Quart. J. Roy. Meteor. Soc.,* **124,** 949–981.

Pan, H. L., and L. Mahrt, 1987: Interaction between soil hydrology and boundary layer developments. *Bound.-Layer Meteor.,* **38,** 185–202.

Paulson, C. A., 1970: Mathematical representation of wind speed and temperature profiles in the unstable atmospheric surface layer. *J. Appl. Meteor.,* **9,** 857–861.

Pitman, A. J., and A. Henderson-Sellers, 1998: Recent progress and results from the project for the intercomparison of land surface parameterization schemes. *J. Hydrol.,* **212-213,** 128–135.

Rayner, N. A., C. K. Folland, D. E. Parker, and B. Horton, 1995: A new Global Sea-Ice and Sea Surface Temperature (GISST) data set for 1903–1994 for forcing climate models. Internal Note 69, Hadley Centre, Met Office, 13 pp.

Robock, A., K. V. Vinnikov, C. A. Schlosser, N. A. Speranskaya, and Y. Xue, 1995: Use of Russian soil moisture and meteorological observations to validate soil moisture simulations with biosphere and bucket models. *J. Climate,* **8,** 15–35.

Sato, N., P. J. Sellers, D. A. Randall, E. K. Schneider, J. Shukla, J. L. Kinter III, Y.-T. Hou, and E. Albertazzi, 1989: Effects of implementing the Simple Biosphere Model in a general circulation model. *J. Atmos. Sci.,* **46,** 2757–2782.

Sellers, P. J., Y. Mintz, Y. C. Sud, and A. Dalcher, 1986: A Simple Biosphere Model (SiB) for use within general circulation models. *J. Atmos. Sci.,* **43,** 505–531.

Seneviratne, S. I., D. Lüthi, M. Litschi, and C. Schär, 2006: Land–atmosphere coupling and climate change in Europe. *Nature,* **443,** 205–209.

Shao, Y., and A. Henderson-Sellers, 1996: Validation of soil moisture simulation in land-surface parameterisation schemes with HAPEX data. *Global Planet. Change,* **13,** 11–46.

Shukla, J., and Y. Mintz, 1982: Influence of land-surface evapotranspiration on the earth's climate. *Science,* **215,** 1498–1501.

Snyder, P. K., C. Delire, and J. A. Foley, 2004: Evaluating the influence of different vegetation biomes on the global climate. *Climate Dyn.,* **23,** 279–302.

Suarez, M. J., A. Arakawa, and D. A. Randall, 1983: The parameterization of the planetary boundary layer in the UCLA general circulation model: Formulation and results. *Mon. Wea. Rev.,* **111,** 2224–2243.

Sud, Y. C., and M. J. Fennessy, 1982: A study of the influence of surface albedo on July circulation in semi-arid regions using the GLAS GCM. *J. Climatol.,* **2,** 105–125.

——, J. Shukla, and Y. Mintz, 1988: Influence of land surface roughness on atmospheric circulation and precipitation: A sensitivity study with a general circulation model. *J. Appl. Meteor.,* **27,** 1036–1054.

Wang, G., and E. A. B. Eltahir, 2000: Biosphere–atmosphere interactions over West Africa. I: Development and validation of a coupled dynamic model. *Quart. J. Roy. Meteor. Soc.,* **126,** 1239–1260.

——, ——, J. A. Foley, D. Pollard, and S. Levis, 2004: Decadal variability of rainfall in the Sahel: Results from the coupled GENESIS-IBIS atmosphere-biosphere model. *Climate Dyn.,* **22,** 625–637, doi:10.1007/s00382-004-0411-3.

Xie, P., and P. A. Arkin, 1997: Global precipitation: A 17-year monthly analysis based on gauge observations, satellite estimates, and numerical model outputs. *Bull. Amer. Meteor. Soc.,* **78,** 2539–2558.

Xue, Y., 1996: The impact of desertification in the Mongolian and the Inner Mongolian grassland on the regional climate. *J. Climate,* **9,** 2173–2189.

——, 1997: Biosphere feedback on regional climate in tropical North Africa. *Quart. J. Roy. Meteor. Soc.,* **123,** 1483–1515.

——, 2005: Land surface processes and monsoon. *GEWEX News,* Vol. 15, International GEWEX Project Office, Silver Spring, MD, 5–6.

——, and J. Shukla, 1993: The influence of land surface properties on Sahel climate. Part I: Desertification. *J. Climate,* **6,** 2232–2245.

——, P. J. Sellers, J. L. Kinter, and J. Shukla, 1991: A simplified biosphere model for global climate studies. *J. Climate,* **4,** 345–364.

——, F. J. Zeng, and C. A. Schlosser, 1996: SSiB and its sensitivity to soil properties—A case study using HAPEX-Mobilhy data. *Global Planet. Change,* **13,** 183–194.

——, ——, K. E. Mitchell, Z. Janjic, and E. Rogers, 2001: The impact of land surface processes on simulations of the U.S. hydrological cycle: A case study of the 1993 flood using the SSiB land surface model in the NCEP Eta regional model. *Mon. Wea. Rev.,* **129,** 2833–2860.

——, S. Sun, D. Kahan, and Y. Jiao, 2003: The impact of parameterizations in snow physics and interface processes on the simulation of snow cover and runoff at several cold region sites. *J. Geophys. Res.,* **108,** 8859, doi:10.1029/2002JD003174.

——, and Coauthors, 2004a: The Sahelian climate. *Vegetation, Water, Humans and the Climate,* Springer-Verlag, 59–77.

——, H.-M. Juang, W.-P. Li, S. Prince, R. DeFries, Y. Jiao, and R. Vasic, 2004b: Role of land surface processes in monsoon development: East Asia and West Africa. *J. Geophys. Res.,* **109,** D03105, doi:10.1029/2003JD003556.

——, F. De Sales, W.-P. Li, C. R. Mechoso, C. A. Nobre, and H.-M. Juang, 2006: Role of land surface processes in South American monsoon development. *J. Climate,* **19,** 741–762.

Yasunari, T., K. Saito, and K. Takata, 2006: Relative roles of large-scale orography and land surface processes in the global hydroclimate. Part I: Impacts on monsoon systems and the tropics. *J. Hydrometeor.,* **7,** 626–641.

Yu, J. Y., and C. R. Mechoso, 2001: A coupled atmosphere–ocean GCM study of the ENSO cycle. *J. Climate,* **14,** 2329–2350.

Zeng, N., J. D. Neelin, K.-M. Lau, and C. J. Tucker, 1999: Enhancement of interdecadal climate variability in the Sahel by vegetation interaction. *Science,* **286,** 1537–1540.

Zhao, M., A. Pitman, and T. Chase, 2001: The impact of land cover change on the atmospheric circulation. *Climate Dyn.,* **17,** 467–477.